SANDIA REPORT

SAND2018-1392
Unlimited Release
Printed February 7, 2018

The Finite Strain Johnson Cook Plasticity and Damage Constitutive Model in ALEGRA

J.J. Sanchez

Prepared by
Sandia National Laboratories
Albuquerque, New Mexico 87185 and Livermore, California 94550

Sandia National Laboratories is a multimission laboratory managed and operated by National Technology and Engineering Solutions of Sandia, LLC, a wholly owned subsidiary of Honeywell International, Inc., for the U.S. Department of Energy's National Nuclear Security Administration under contract DE-NA0003525.
Approved for public release; further dissemination unlimited.

Issued by Sandia National Laboratories, operated for the United States Department of Energy by National Technology and Engineering Solutions of Sandia, LLC.

Available to DOE and DOE contractors from
U.S. Department of Energy
Office of Scientific and Technical Information
P.O. Box 62
Oak Ridge, TN 37831

Telephone: (865) 576-8401
Facsimile: (865) 576-5728
E-Mail: reports@adonis.osti.gov
Online ordering: http://www.osti.gov/bridge

Available to the public from
U.S. Department of Commerce
National Technical Information Service
5285 Port Royal Rd
Springfield, VA 22161

Telephone: (800) 553-6847
Facsimile: (703) 605-6900
E-Mail: orders@ntis.fedworld.gov
Online ordering: http://www.ntis.gov/help/ordermethods.asp?loc=7-4-0#online

SAND2018-1392
Unlimited Release
Printed February 7, 2018

The Finite Strain Johnson Cook Plasticity and Damage Constitutive Model in ALEGRA

Jason J. Sanchez
Computational Shock and Multiphysics
Sandia National Laboratories
Albuquerque, NM 87185-1323
jassanc@sandia.gov

Abstract

A finite strain formulation of the Johnson Cook plasticity and damage model and it's numerical implementation into the ALEGRA code is presented. The goal of this work is to improve the predictive material failure capability of the Johnson Cook model. The new implementation consists of a coupling of damage and the stored elastic energy as well as the minimum failure strain criteria for spall included in the original model development. This effort establishes the necessary foundation for a thermodynamically consistent and complete continuum solid material model, for which all intensive properties derive from a common energy. The motivation for developing such a model is to improve upon ALEGRA's present combined model framework. Several applications of the new Johnson Cook implementation are presented. Deformation driven loading paths demonstrate the basic features of the new model formulation. Use of the model produces good comparisons with experimental Taylor impact data. Localized deformation leading to fragmentation is produced for expanding ring and exploding cylinder applications.

Acknowledgment

This work was supported by the U.S. Army Research Laboratory and DOE's National Nuclear Security Administration. The author also gratefully acknowledges the consultation provided by Bill Scherzinger, Jakob Ostien, John Carpenter and Ed Love.

Contents

Appendix

Figures

Tables

1 Introduction

The phenomenological continuum solid mechanics plasticity and damage models developed by Johnson and Cook [1, 2] are among the most extensively used by computational physics codes to simulate high loading rate applications. Users of the ALEGRA multi-physics multi-material finite element code [3, 4] rely heavily on the Johnson Cook model to provide predictions of plastic material behavior and material failure. A high degree of success has been achieved using the Johnson Cook models in ALEGRA to represent material response for shock and solid dynamics applications at an engineering scale. Despite this success, the ability to consistently reproduce physically realistic material failure results remains elusive.

The source of this issue could be attributed to the validity of the model itself, potential inadequacies of the model's numerical implementation or a combination of both. This work focuses solely on improvements to the implementation of the Johnson Cook model given any of its shortcomings for predicting material behavior. The current implementation of the Johnson Cook damage model is treated as an afterthought in ALEGRA's combined material model framework [4]. This is because the damage evolution equation is not coupled to the evaluation of the Johnson Cook plasticity model, which in the opinion of the author, is the proper treatment. Instead, the damage model is evaluated independently and its result is used as a criterion for the initiation of the material failure process that is teated by a completely different model. This algorithmic treatment of damage models is questionable in general, and motivates the development of a new implementation founded on a continuum formulation that includes the simultaneous evolution of both plasticity and damage as well as the associated degradation of the material's load carrying capacity.

ALEGRA's combined model framework preforms a careful series of different material model evaluations that are generally based on the spherical and deviatoric splitting of the stress tensor. In general, the pressure is obtained from an equation of state (EOS) and the stress deviator is obtained from the evaluation of a continuum plasticity model (i.e. Johnson Cook plasticity) along with plastic strain history variables. An infinitesimal (small) strain formulation based on isotropic linear elasticity is assumed for the plasticity model and any contribution to the pressure from the plasticity model solution is discarded and replaced with the value predicted by the EOS. Since an EOS is not generally equipped to handle tensile pressure states, the evaluation of a void insertion model within the combined model framework has proved necessary. Once a material is loaded to a tensile failure pressure, this model controls the volume fraction of void (empty space) at the individual cell level by adjusting material density as the pressure is reduced to zero over time. The intended effect is the loss of tensile load carrying capability, material separation and mitigation of tensile states predicted by the EOS, which are generally constructed in an ad hoc fashion and are prone to prediction of unphysical material states. If material failure modeling is desired, then a damage model (i.e. Johnson Cook damage) is applied on top of this framework. The evolution of the damage history variable is evaluated independently, uncoupled from the plasticity model. Degradation of the stress is not initiated until a material is completely damaged (damage has a value of one). At this point, degradation is controlled by the void insertion model that reduces the tensile failure pressure to a zero value over a certain number of computational cycles. The stress deviator

is degraded similarly. An inconsistency lies in the fact that the void insertion tensile pressure failure criterion and the complete evolution of damage dictated by the Johnson Cook damage model do not necessarily coincide. Typically, a damage variable is coupled to the constitutive model equations through the degradation of stress or elastic parameters. However, this is not the case in ALEGRA's combined model implementation, for which the damage variable does not actually produce any degradation. In addition, the tensile failure pressure criterion differs from the minimum failure strain criterion that is actually used in the original development of the model [2].

The immediate objective of the present work is to improve the predictive material failure capability of the Johnson Cook model. A new implementation of the Johnson Cook plasticity and damage model in ALEGRA is preformed in order to achieve this goal, and attempt to offer fundamental improvements to the overall aforementioned combined material model framework. A finite strain formulation of the model is utilized that includes coupling between damage and the stored elastic energy as well as the minimum failure strain criterion for spall included in the original work [2]. This approach has several advantages. First, the finite strain deformation framework properly incorporates the geometric nonlinearities associated with large deformation continuum mechanics, appropriate for the intended applications. The natural incorporation of hyperelasticity into the finite strain formulation explicitly provides a stored energy function, from which the intensive material variables (i.e. stress, temperature, etc.) are derived. This feature sets the constitutive model on the same theoretical continuum thermodynamic footing as equation of state models. An adequate framework is provided that can produce a consistent thermodynamic material state for solids that includes the stress and history variables. Such a framework could potentially eliminate need for the spherical and deviatoric splitting of the stress tensor that is currently necessitated by the evaluation of EOS and solid constitutive models that produce inconsistent pressure states, as well as ad hoc treatment of tensile states in the EOS models. The application of some of these ideas can be found in references [5, 6, 7, 8, 9, 10]. The coupling of the damage history variable to the elastic stored energy results in damaged material states that reflect a loss of load carrying capability rather than the current uncoupled approach that only uses damage as a failure initiation criterion for another model (i.e. void insertion).

This work focuses on solid material states predicted only by the Johnson Cook constitutive model, in particular those leading to material failure. The incorporation of a complete thermodynamic state remains as future work. The new Johnson Cook implementation is applied to a range of applications. Simple loading paths demonstrate the basic capabilities. Taylor impact problem results for plasticity compare well to experimental data. Expending ring and exploding cylinder problems then demonstrate examples of localized damage and fragmentation that are intuitively expected for such applications. This report is organized as follows. Section 2 summarizes isotropic continuum finite strain plasticity. A computational solution method is presented in Section 3. The Johnson Cook plasticity and damage models, their computational approaches and implementation details are then presented in Section 4. Results for several applications are then presented in Section 5. Finally conclusions are discussed and future work efforts are identified in Section 6.

2 Summary of Continuum Finite Strain Plasticity

The continuum equations for finite strain plasticity presented in this section are based on references [11] and [12]. The discussion is restricted to the continuum solid material constitutive (closure) model that relates the deformation to the stress tensor at a single point in the material. The stress is the essential quantity required for evaluation of the internal force contribution to the conservation of linear momentum. The four elements that generally define inelastic constitutive models are discussed. These elements are the kinematics, elasticity, plastic yield criterion and plastic flow evolution.

2.1 Kinematics

Consider a point in a solid continuum body, $\mathbf{X}$, in its initial undeformed state. Let $\mathbf{x}$ denote the position of that same material point in the final deformed configuration of the solid body. There exists a unique mapping, $\mathbf{x} = \mathbf{x}(\mathbf{X})$, relating the initial and final positions of the material point. The deformation gradient $\mathbf{F}$ is a second order tensor defined as follows:

$$\mathbf{F} = \frac{d\mathbf{x}}{d\mathbf{X}} \tag{1}$$

The deformation gradient is the fundamental deformation measure from which all other deformation measures (strains) are derived, including the infinitesimal (small) strain approximation. It provides the transformation between deformed ($\mathbf{dx}$) and undeformed ($\mathbf{dX}$) line segments of material; $\mathbf{dx} = \mathbf{F} \cdot \mathbf{dX}$ and $\mathbf{dX} = \mathbf{F}^{-1} \cdot \mathbf{dx}$. The elastic and plastic contributions to a deformation are defined by the following multiplicative decomposition of $\mathbf{F}$.

$$\mathbf{F} = \mathbf{F}^e \cdot \mathbf{F}^p \tag{2}$$

The superscripts e and p are used to denote kinematic quantities associated with elastic and plastic deformations respectively. Given the definition in equation (2), the deformation measures relevant to the development of the finite strain plasticity equations and their solution algorithms will be defined. The left polar decomposition of $\mathbf{F}$ is

$$\mathbf{F} = \mathbf{V} \cdot \mathbf{R} \tag{3}$$

where $\mathbf{V} = \mathbf{V}^T$ and $\mathbf{R}^{-1} = \mathbf{R}^T$. The elastic and plastic deformation gradients are decomposed similarly.

$$\mathbf{F}^e = \mathbf{V}^e \cdot \mathbf{R}^e \tag{4}$$

$$\mathbf{F}^p = \mathbf{V}^p \cdot \mathbf{R}^p \tag{5}$$

The left Cauchy-Green tensor, $\mathbf{b}$, and the elastic left Cauchy-Green tensor, $\mathbf{b}^e$ are defined as follows:

$$\mathbf{b} = \mathbf{F} \cdot \mathbf{F}^T = \mathbf{V}^2 \tag{6}$$

$$\mathbf{b}^e = \mathbf{F}^e \cdot \mathbf{F}^{eT} = \mathbf{V}^{e2} \tag{7}$$

The right Cauchy-Green tensor, $\mathbf{C}$ is

$$\mathbf{C} = \mathbf{F}^T \cdot \mathbf{F} \tag{8}$$

and the inverse plastic right Cauchy-Green tensor is

$$\mathbf{C}^{p-1} = \mathbf{F}^{p-1} \cdot \mathbf{F}^{p-T} = \mathbf{F}^{-1} \cdot \mathbf{b}^e \cdot \mathbf{F}^{-T} \tag{9}$$

The logarithmic strain tensor, ε and elastic logarithmic strain tensor, ε^e are

$$\varepsilon = \frac{1}{2}\ln(\mathbf{b}) \tag{10}$$

$$\varepsilon^e = \frac{1}{2}\ln(\mathbf{b}^e) \tag{11}$$

Volumetric deformations are defined in terms of the quantity, $J > 0$, defined as follows:

$$J = \det(\mathbf{F}) = \det(\mathbf{F}^e)\det(\mathbf{F}^p) = J^e J^p \tag{12}$$

This development assumes isochoric plastic deformation, which places the following restrictions on the elastic and plastic contributions of J.

$$J^p = 1 \qquad J^e = J \tag{13}$$

The isochoric elastic left Cauchy-Green tensor, $\bar{\mathbf{b}}^e$, defined below, has a determinant value of 1.

$$\bar{\mathbf{b}}^e = J^{e-\frac{2}{3}}\mathbf{b}^e \tag{14}$$

The following relationship should also be noted.

$$\ln(J^e) = tr(\varepsilon^e) \tag{15}$$

Let $\mathbf{L}$ denote the velocity gradient. Two expressions for $\mathbf{L}$ are

$$\mathbf{L} = \dot{\mathbf{F}} \cdot \mathbf{F}^{-1} = \mathbf{D} + \mathbf{W} \tag{16}$$

where a superimposed dot denotes a material time derivative, $\mathbf{D}$ is the deformation rate (symmetric part of the velocity gradient) and $\mathbf{W}$ is the spin (antisymmetric part of the velocity gradient). The plastic velocity gradient is

$$\mathbf{L}^p = \dot{\mathbf{F}}^p \cdot \mathbf{F}^{p\,-1} = \mathbf{D}^p + \mathbf{W}^p \tag{17}$$

The plastic deformation is also assumed to be irrotational, which results in the following simplification.

$$\mathbf{W}^p = \mathbf{0} \tag{18}$$

2.2 Isotropic Hyperelasticity

Consider an isotropic hyperelastic (Hemholtz) stored energy function, Ψ, of an elastic deformation measure as follows:

$$\Psi = \Psi(\mathbf{F}^e) = \Psi(\mathbf{b}^e) = \Psi(\varepsilon^e) \tag{19}$$

The quantity, Ψ represents energy per unit reference (initial) volume. It is split into volumetric and deviatoric contributions denoted by the superscripts *vol* and *dev* respectively. Split representations of Ψ in terms of $\mathbf{b^e}$ and ε^e are

$$\Psi(\mathbf{b}^e) = \Psi^{vol}(J^e) + \Psi^{dev}(\bar{\mathbf{b}}^e) \tag{20}$$

and

$$\Psi(\varepsilon^e) = \Psi^{vol}(J^e) + \Psi^{dev}(\varepsilon^{e\,dev}) \tag{21}$$

where

$$\varepsilon^{e\,dev} = \varepsilon^e - \frac{1}{3} tr(\varepsilon^e)\mathbf{I} \tag{22}$$

The stress tensor is derived from the elastic stored energy. The Kirchhoff stress definition is

$$\tau = \frac{\partial \Psi}{\partial \mathbf{F}^e} \cdot \mathbf{F}^{e\,T} = 2\frac{\partial \Psi}{\partial \mathbf{b}^e} \cdot \mathbf{b}^e = \frac{\partial \Psi}{\partial \varepsilon^e} \tag{23}$$

and the Cauchy stress is obtained from the following relationship.

$$\sigma = J\tau \tag{24}$$

A commonly used Neo Hookean model is

$$\Psi(\mathbf{b}^e) = \frac{\kappa}{2}\left(\frac{1}{2}(J^{e\,2} - 1) - \ln(J^e)\right) + \frac{\mu}{2}\left(\bar{\mathbf{b}}^e : \mathbf{I} - 3\right) \tag{25}$$

where κ is the bulk modulus and μ is the shear modulus. It can be shown, using the definition in equation (23), that the Kirchhoff stress associated with the Neo Hookean form of stored energy in equation (25) is

$$\tau = \frac{\kappa}{2}(J^{e\,2} - 1)\mathbf{I} + \mu J^{e\,-\frac{2}{3}}\mathbf{b}^{e\,dev} \tag{26}$$

The isotropic nature of the scalar hyperelastic energy function $\Psi(\mathbf{F}^e)$ plays an important role in the algorithmic developments that follow. Isotropy of Ψ with respect to the tensor $\mathbf{F}^e$ means that the value of Ψ is independent of orthogonal transformations of $\mathbf{F}^e$ such that $\Psi(\mathbf{F}^e) = \Psi(\mathbf{Q} \cdot \mathbf{F}^e \cdot \mathbf{Q}^T)$ for all rotation tensors, $\mathbf{Q}$ ($\mathbf{Q}^{-1} = \mathbf{Q}^T$). An important consequence of isotropy is the resulting coaxial relationship between the tensor argument, $\mathbf{b}^e$, and the derivative of the isotropic function with respect to the tensor argument, $\partial\Psi/\partial\mathbf{b}^e$. The coaxial tensors, $\mathbf{b}^e$ and $\partial\Psi/\partial\mathbf{b}^e$, share the same principal basis, and consequently commute with each other. In the case of $\Psi(\mathbf{b}^e) = \Psi(\varepsilon^e)$, the following relationships hold

$$\mathbf{b}^e \cdot \frac{\partial \Psi}{\partial \mathbf{b}^e} = \frac{\partial \Psi}{\partial \mathbf{b}^e} \cdot \mathbf{b}^e \qquad \varepsilon^e \cdot \frac{\partial \Psi}{\partial \varepsilon^e} = \frac{\partial \Psi}{\partial \varepsilon^e} \cdot \varepsilon^e \tag{27}$$

The following important result is easily obtained by inspection of equations (23) and (27).

$$\mathbf{b}^e \cdot \tau = \tau \cdot \mathbf{b}^e \qquad \varepsilon^e \cdot \tau = \tau \cdot \varepsilon^e \tag{28}$$

2.3 Plastic Yield

The isotropic yield surface function, $F = F(\tau, \alpha)$ defines the elastic limit in stress space, for which the quantity, α, represents a set of history variables. The criterion for plastic deformation is

$$\begin{array}{ll} F(\tau,\alpha) < 0 & \text{elastic behavior} \\ F(\tau,\alpha) = 0 & \text{evolution of plastic flow (consistency condition)} \\ F(\tau,\alpha) > 0 & \text{not permitted (indication that plasticity needs to evolve)} \end{array} \tag{29}$$

A common isotropic plasticity model is the J_2 plasticity model with hardening. The associated yield function is

$$F(\tau, \bar{\varepsilon}) = \bar{\tau} - Y(\bar{\varepsilon}) \tag{30}$$

where Y is the hardening function, $\bar{\varepsilon}$ is the scalar equivalent plastic strain history variable and $\bar{\tau}$ is the Von Mises stress, defined as follows:

$$\bar{\tau} = \left(\frac{3}{2} \tau^{dev} : \tau^{dev} \right)^{\frac{1}{2}} \tag{31}$$

It is important to note the isotropy of $F = F(\tau, \alpha)$ with respect to τ. As a result, $F(\tau, \alpha) = F(\mathbf{Q} \cdot \tau \cdot \mathbf{Q}^T, \alpha)$ and the following coaxial relationship holds (see discussion in section 2.2).

$$\frac{\partial F}{\partial \tau} \cdot \tau = \tau \cdot \frac{\partial F}{\partial \tau} \tag{32}$$

2.4 Evolution of Plastic Flow

The evolution of the rotated plastic deformation rate is assumed to follow an associative flow rule defined in [11] as follows :

$$\mathbf{R}^e \cdot \mathbf{D}^p \cdot \mathbf{R}^{eT} = \dot{\lambda} \frac{\partial F}{\partial \tau} \tag{33}$$

The consistency variable, λ, is a monotonically increasing quantity requiring that

$$\dot{\lambda} \geq 0 \tag{34}$$

The combination of the kinematic relationships in equations (17) and (18) and equation (33) give the following result for the evolution of the plastic deformation gradient.

$$\dot{\mathbf{F}}^p = \dot{\lambda}\mathbf{R}^{eT} \cdot \frac{\partial F}{\partial \tau} \cdot \mathbf{R}^e \cdot \mathbf{F}^p \tag{35}$$

The evolution of history variables is assumed to have a similar form to that of equation (33).

$$\dot{\alpha} = \dot{\lambda}\mathbf{h} \tag{36}$$

The typically assumed form of $\mathbf{h}$ is

$$\mathbf{h} = \frac{\partial F}{\partial \alpha} \tag{37}$$

Lastly, important relationships, established for future reference, are direct results of isotropy of both $\Psi(\mathbf{b}^e)$ and $F(\tau, \alpha)$. Combination of the elastic and plastic isotropy relationships in equations (28) and (32) and the kinematic relationship in equation (7) provides the following results to be used in later algorithmic developments:

$$\frac{\partial F}{\partial \tau} \cdot \mathbf{b}^e = \mathbf{b}^e \cdot \frac{\partial F}{\partial \tau} \tag{38}$$

$$\frac{\partial F}{\partial \tau} \cdot \mathbf{V}^e = \mathbf{V}^e \cdot \frac{\partial F}{\partial \tau} \tag{39}$$

2.5 Summary of Finite Strain Plasticity Equations

In summary, the development of the finite strain plasticity equations assume isotropy of the hyperelastic stored energy function Ψ and the plastic yield function, F. Associativity of the plastic deformation rate evolution is also assumed. Given these assumptions, the finite strain plasticity equations are provided below and utilized in the algorithmic development of the following section.

$$
\begin{aligned}
&\mathbf{F} = \mathbf{F}^e \cdot \mathbf{F}^p && \text{finite strain elastic-plastic kinematics} \\
&\tau = \frac{\partial \Psi}{\partial \mathbf{F}^e} \cdot \mathbf{F}^{eT} && \text{elasticity} \\
&F(\tau, \alpha) = 0 && \text{consistency condition} \\
&\dot{\mathbf{F}}^p = \dot{\lambda} \mathbf{R}^{eT} \cdot \frac{\partial F}{\partial \tau} \cdot \mathbf{R}^e \cdot \mathbf{F}^p && \text{evolution of plastic flow} \\
&\dot{\alpha} = \dot{\lambda} \mathbf{h} && \text{history variable evolution}
\end{aligned}
\tag{40}
$$

3 A Computational Method for Finite Strain Plasticity

This section summarizes a general elastic predictor algorithm for obtaining a solution to the time-discretized system of equations in (40). Consider the equations in (40) to be an initial value problem for which initial problem data is known. Let the superscript n denote a discrete time index indicating the value of a quantity at discrete time t^n. Given the initial data at time t^n, the solution at time $t^{n+1} = t^n + \Delta t$ is sought. Specifically, the initial values for Kirchhoff stress τ^n, inverse plastic right Cauchy-Green tensor, $\mathbf{C}^{p-1\,n}$ and the history variables α^n are available and τ^{n+1}, $\mathbf{C}^{p-1\,n+1}$ and α^{n+1} are the desired solutions. The choice of using $\mathbf{C}^{p-1\,n+1}$ as the plastic deformation measure of interest is based mostly on convenience from an algorithmic perspective, which will become clear later. It is also assumed that the updated deformation gradient $\mathbf{F}^{n+1}$ is known. The previously computed update is

$$\mathbf{F}^{n+1} = \Delta\mathbf{F} \cdot \mathbf{F}^n \tag{41}$$

where the incremental deformation gradient ,$\Delta\mathbf{F}$, is applied.

The solution algorithm requires the evaluation of a trial state for which the incremental deformation is assumed to be elastic. The trial elastic deformation gradient at t^{n+1} is

$$\mathbf{F}^{etr} = \Delta\mathbf{F} \cdot \mathbf{F}^{en} \tag{42}$$

where the superscript tr indicates an elastic trial value of a quantity. It follows that an alternative expression for $\mathbf{F}^{n+1}$ in terms of the elastic trial state is

$$\mathbf{F}^{n+1} = \mathbf{F}^{etr} \cdot \mathbf{F}^{pn} \tag{43}$$

The value for $\mathbf{b}^{etr}$ is

$$\mathbf{b}^{etr} = \Delta\mathbf{F} \cdot \mathbf{b}^{en} \cdot \Delta\mathbf{F}^T = \mathbf{F}^{etr} \cdot \mathbf{F}^{etrT} \tag{44}$$

Use of equations (9) and (42) lead to the following alternative expression for $\mathbf{b}^{etr}$ stated here for future reference.

$$\mathbf{b}^{etr} = \mathbf{F}^{n+1} \cdot \mathbf{C}^{p-1\,n} \cdot \mathbf{F}^{n+1\,T} \tag{45}$$

Computation of ε^{etr} is obtained from equation (11)

$$\varepsilon^{etr} = \frac{1}{2}\ln(\mathbf{b}^{etr}) \tag{46}$$

The trial stress computed for the elastic trial state is

$$\tau^{tr} = \frac{\partial \Psi}{\partial \varepsilon^e}(\varepsilon^{etr}) \tag{47}$$

The plastic yield function is evaluated at the trial state as $F^{tr} = F(\tau^{tr}, \alpha^n)$. If $F^{tr} < 0$, then the deformation is completely elastic and the trivial material state is update is

$$\begin{aligned} \tau^{n+1} &= \tau^{tr} \\ \mathbf{C}^{p-1\,n+1} &= \mathbf{C}^{p-1\,n} \\ \alpha^{n+1} &= \alpha^n \end{aligned} \tag{48}$$

If $F^{tr} >= 0$, then plastic flow must evolve in order to satisfy the time-discretized system of equations in (40).

The key component of this solution algorithm is the time integration of the plastic flow evolution equation in (35), restated below for convenience.

$$\dot{\mathbf{F}}^p = \dot{\lambda}\mathbf{R}^{eT} \cdot \frac{\partial F}{\partial \tau} \cdot \mathbf{R}^e \cdot \mathbf{F}^p$$

Given the initial data, $\mathbf{F}^{pn}$, equation (35) is integrated over time increment $\Delta t = t^{n+1} - t^n$ using a backward (fully implicit) exponential map. The result is

$$\mathbf{F}^{pn+1} = \exp\left[\Delta t \dot{\lambda}\mathbf{R}^{eT\,n+1} \cdot \left(\frac{\partial F}{\partial \tau}\right)^{n+1} \cdot \mathbf{R}^{en+1}\right] \cdot \mathbf{F}^{pn} \tag{49}$$

It can be shown that the result in equation (49) reduces to the following logarithmic strain update. Details of the derivation, found in Appendix A, rely heavily on isotropy of the stored energy and yield function and the resulting coaxial relationships in equations (38) and (39).

$$\varepsilon^{en+1} = \varepsilon^{etr} - \Delta\lambda \left(\frac{\partial F}{\partial \tau}\right)^{n+1} \tag{50}$$

The result in equation (50) is nearly identical to the form of the incremental plastic strain update used for infinitesmal strain plasticity. The incremental evolution of the history variables is

$$\Delta\alpha = \Delta\lambda \mathbf{h}^{n+1} \tag{51}$$

and the history variable update is

$$\alpha^{n+1} = \alpha^n + \Delta\alpha \tag{52}$$

The updated stress is computed as follows:

$$\tau^{n+1} = \frac{\partial \Psi}{\partial \varepsilon^e}(\varepsilon^{en+1}) \tag{53}$$

The finial material state at t^{n+1} must also satisfy the consistency condition.

$$F(\tau^{n+1}, \alpha^{n+1}) = 0 \tag{54}$$

In summary, if the trial state based on equations (42)-(47) result in a trial yield function value $F^{tr} = F(\tau^{tr}, \alpha^n) > 0$ then plastic flow must evolve in order to solve the following time-discretized system of nonlinear equations for finite strain plasticity for the updated state defined by τ^{n+1}, $\mathbf{C}^{p-1\,n+1}$ and α^{n+1}:

$$\begin{aligned}
&F(\tau^{n+1}, \alpha^{n+1}) = 0 \\
&\tau^{n+1} = \frac{\partial \Psi}{\partial \varepsilon^e}(\varepsilon^{en+1}) \\
&\varepsilon^{en+1} = \varepsilon^{etr} - \Delta\lambda \left(\frac{\partial F}{\partial \tau}\right)^{n+1} \\
&\Delta\alpha = \Delta\lambda \mathbf{h}^{n+1} \\
&\alpha^{n+1} = \alpha^n + \Delta\alpha
\end{aligned} \tag{55}$$

Once the solution is obtained for the system in equation (55), the value of $\mathbf{C}^{p-1\,n+1}$ is obtained through the following series of operations:

$$\mathbf{b}^{en+1} = \exp\left(2\varepsilon^{en+1}\right) \tag{56}$$

$$\mathbf{C}^{p-1\,n+1} = \mathbf{F}^{n+1\,-1} \cdot \mathbf{b}^{en+1} \cdot \mathbf{F}^{n+1\,-T} \tag{57}$$

Typically the updated solution for the Cauchy stress, σ^{n+1} , is required.

$$\boldsymbol{\sigma}^{n+1} = \frac{1}{J^{n+1}} \boldsymbol{\tau}^{n+1} \tag{58}$$

The updated deformation gradient determinant, J^{n+1}, is

$$J^{n+1} = \det\left(\mathbf{F}^{n+1}\right) \tag{59}$$

The use of the particular finite strain plasticity solution algorithm outlined in this section has several advantages. One advantage is that it is easily adaptable from existing small strain plasticity solution algorithms due to the additive nature of the elastic logarithmic strain measure utilized. The elastic and plastic isotropy properties provide other computational advantages. Obviously, the development of the algorithm itself relies on these properties. Since isotropy dictates that $\mathbf{b}^{en+1}$ and $\boldsymbol{\tau}^{n+1}$ share the same principal bases, the solution procedure for the nonlinear system in equation (55) can be performed with respect to stress and strain components in that common principal basis. This convenient property provides a computational cost savings that allows for a minimal set of equations (unknowns) to be solved in (55). The eigenpair computation of $\mathbf{b}^{etr}$ need only be performed once prior to the solution procedure. Once the solution to the principal values of $\mathbf{b}^{en+1}$ and $\boldsymbol{\tau}^{n+1}$ are obtained, their representations in the problem basis are reconstructed from the eigenvectors. The initial eigenpair solution is necessary anyway in order to perform the second order tensor natural log and exponentiation operations to obtain $\boldsymbol{\varepsilon}^{etr}$ and $\mathbf{b}^{en+1}$ respectively. However, it is important to note that the aforementioned advantages are precluded with the introduction of an anisotropic hyperelastic stored energy or yield surface function or a non-associative plastic flow relationship. In either case, the coaxial relationships established in equations (38) and (39) would no longer be valid, requiring development of a different solution algorithm.

4 The Johnson Cook Finite Strain Constitutive Model

The finite strain formulation of the Johnson-Cook plasticity and damage models is presented. The continuum model is defined first, followed by the numerical algorithm which is implemented into the ALEGRA multi-physics code. Computational aspects of the implementation specific to the ALEGRA code are discussed separately.

4.1 The Johnson-Cook Plasticity and Damage Models

The original work of Johnson and Cook for modeling plasticity and damage of metals is found in [1] and [2] respectively. The Johnson-Cook models are highly utilized in computational physics codes, including ALEGRA, for the simulation of high loading rate solid dynamics and shock applications. The simplicity of a relatively small parameter space along with the availability of extensive model parameterizations [13] and validation efforts [14] have made the model very attractive to users.

The finite strain formulation of the Johnson Cook plasticity model is developed first using the framework presented Section 2. Equation (40) summarizes this framework. Johnson-Cook plasticity utilizes the J_2 yield function form of $F(\tau,\bar{\varepsilon})$ in equation (30), restated below.

$$F(\tau,\bar{\varepsilon}) = \bar{\tau} - Y(\bar{\varepsilon})$$

The specific form of the hardening function ([1]), which incorporates dependence on plastic strain rate and temperature, is

$$Y(\bar{\varepsilon}) = \left[A + B\bar{\varepsilon}^N\right]\left[1 + C\ln\left(\dot{\bar{\varepsilon}}\right)\right]\left[1 - \theta^M\right] \tag{60}$$

where A, B, C, N and M are model parameters, $\dot{\bar{\varepsilon}}$ is the plastic strain rate and the homologous temperature, θ is defined as follows:

$$\theta = \frac{T - T_r}{T_M - T_r} \tag{61}$$

The quantities T, T_M and T_r are the material temperature, melt temperature and room temperature respectively. The equivalent plastic strain, $\bar{\varepsilon}$, is the single scalar history variable subject to the following evolution relationship.

$$\dot{\bar{\varepsilon}} = \dot{\lambda} h \tag{62}$$

Equations (30), (60)-(62) and the set of equations in (40) are combined to form the following Johnson-Cook finite strain plasticity model.

$$
\begin{aligned}
&\mathbf{F} = \mathbf{F}^e \cdot \mathbf{F}^p && \text{finite strain elastic-plastic kinematics}\\
&\tau = \frac{\partial \Psi}{\partial \mathbf{F}^e} \cdot \mathbf{F}^{eT} && \text{elasticity}\\
&F(\tau, \bar{\varepsilon}) = \bar{\tau} - \left[A + B\bar{\varepsilon}^N\right]\left[1 + C\ln\left(\dot{\bar{\varepsilon}}\right)\right]\left[1 - \theta^M\right] = 0 && \text{consistency condition}\\
&\dot{\mathbf{F}}^p = \dot{\lambda}\mathbf{R}^{eT} \cdot \frac{\partial F}{\partial \tau} \cdot \mathbf{R}^e \cdot \mathbf{F}^p && \text{evolution of plastic flow}\\
&\dot{\bar{\varepsilon}} = \dot{\lambda} h && \text{equivalent plastic strain evolution}
\end{aligned}
\tag{63}
$$

The Johnson-Cook damage model is obtained by introducing a scalar damage history variable, D, and its associated evolution equation into the set of equations for finite strain plasticity in (63). The damage quantity is bounded such that $0 \leq D \leq 1$. A damage value of $D = 0$ indicates undamaged material and a value of $D = 1$ indicates completely damaged material that has lost load carrying capacity. The Johnson Cook damage evolution equation, taken from [2], is

$$\dot{D} = \frac{\dot{\bar{\varepsilon}}}{\varepsilon^f} \tag{64}$$

The failure strain, ε^f, is

$$
\varepsilon^f = \begin{cases} \left[D_1 + D_2 e^{D_3 \sigma^*}\right]\left[1 + D_4 \ln\left(\dot{\varepsilon}^*\right)\right]\left[1 + D_5 \theta\right] & \sigma^* < 1.5 \\ \varepsilon^f_{min} & \sigma^* \geq 1.5 \quad \text{(spall)} \end{cases}
\tag{65}
$$

where D_1, D_2, D_3, D_4, D_5 and ε^f_{min} are model parameters, σ^*, referred to as the triaxial ratio, is

$$\sigma^* = \frac{P}{\bar{\sigma}} \tag{66}$$

where P is the hydrostatic pressure defined as $P = 1/3tr(\sigma)$ and $\bar{\sigma}$ is the Von Mises stress. The quantity $\dot{\varepsilon}^* = \dot{\bar{\varepsilon}}/\dot{\bar{\varepsilon}}_0$ is the dimensionless plastic strain rate for $\dot{\bar{\varepsilon}}_0 = 1$.

The significance of the triaxial ratio value of $\sigma^* = 1.5$ and the discontinuous nature of the failure strain function in equation (65) at that value is based on the assumptions made in the original development work of the Johnson Cook failure model [2]. The value of $\sigma^* = 1.5$ is based on the

approximate material failure mode transition to spall for $\sigma^* \geq 1.5$ observed for the materials of interest. The associated discontinuity of ε^f at $\sigma^* = 1.5$ is due to the assumed constant failure strain treatment of the spall failure process. It is noted that piecewise continuity of ε^f at $\sigma^* = 1.5$ is enforced if the following holds.

$$\varepsilon^f_{min} = \left[D_1 + D_2 e^{D_3 1.5}\right] \left[1 + D_4 \ln\left(\dot{\varepsilon}^*\right)\right] \left[1 + D_5 \theta\right] \tag{67}$$

Two major assumptions are made in the development of the finite strain Johnson Cook damage model with regard to how the damage variable is applied for limiting load carrying capacity of the material. First, is to make the yield function a function of damage as follows:

$$F(\tau, \bar{\varepsilon}, D) = \bar{\tau} - (1 - D) Y(\bar{\varepsilon}) \tag{68}$$

The application of damage in equation (68) has the effect of reducing the deviatoric stress to zero for $D = 1$. The second major assumption is degradation of stored elastic energy due to the evolution of damage. A modified elastic stored energy, $\bar{\Psi} = \bar{\Psi}(\varepsilon^e, D)$, is proposed based on the split volumetric and deviatoric energy contribution form of $\Psi(\varepsilon^e)$ in equation (21). The proposed form of $\bar{\Psi}(\varepsilon^e, D)$ is

$$\bar{\Psi}(\varepsilon^e, D) = \begin{cases} \Psi^{vol}(J^e) + (1 - D)\Psi^{dev}(\varepsilon^{e\,dev}) & \sigma^* < 1.5 \\ \\ (1 - D)\Psi(\varepsilon^e) & \sigma^* \geq 1.5 \quad \text{(spall)} \end{cases} \tag{69}$$

The degradation of elastic stored energy in equation (69) attempts to reduce load carrying capacity of the material in a manner consistent with how the Johnson Cook model distinguishes material failure modes in equation (65). Triaxial states of loading for which $\sigma^* < 1.5$ (which includes compressive states) experience a degradation of only the deviatoric elastic strain energy contribution. Loading states for which $\sigma^* \geq 1.5$ experience a degradation of the total stored energy which allows for a complete degradation of tensile load carrying capacity consistent with spall failure and necessary for modeling the material separation that accompany such events. The stored energy form in equation (69) also allows completely damaged material to retain compressive load carrying capability.

A summary of the finite strain Johnson Cook failure model is

$$
\begin{aligned}
&\mathbf{F} = \mathbf{F}^e \cdot \mathbf{F}^p && \text{finite strain elastic-plastic kinematics}\\
&\tau = \frac{\partial \bar{\Psi}}{\partial \varepsilon^e} \qquad \left(\varepsilon^e = \frac{1}{2}\ln\left(\mathbf{F}^e \cdot \mathbf{F}^{eT}\right)\right) && \text{elasticity}\\
&F(\tau, \bar{\varepsilon}, D) = \bar{\tau} - (1-D)\left[A + B\bar{\varepsilon}^N\right]\left[1 + C\ln\left(\dot{\bar{\varepsilon}}\right)\right]\left[1 - \theta^M\right] = 0 && \text{consistency condition}\\
&\dot{\mathbf{F}}^p = \dot{\lambda}\mathbf{R}^{eT} \cdot \frac{\partial F}{\partial \tau} \cdot \mathbf{R}^e \cdot \mathbf{F}^p && \text{evolution of plastic flow}\\
&\dot{\bar{\varepsilon}} = \dot{\lambda} h && \text{equivalent plastic strain evolution}\\
&\dot{D} = \frac{\dot{\bar{\varepsilon}}}{\varepsilon^f} && \text{damage evolution}
\end{aligned}
\tag{70}
$$

where ε^f and $\bar{\Psi}$ are defined in equations (65) and (69) respectively. The set of equations in (70) can be thought of as two models; one for each triaxial loading range, $\sigma^* < 1.5$ and $\sigma^* \geq 1.5$. Determination of which to use is addressed in the following algorithmic developments.

4.2 Numerical Implementation

Development of the time-discretized systems of equations associated with the continuum finite strain Johnson Cook plasticity and damage models presented in Section 4.1 are based on the general finite deformation plasticity computational framework presented in Section 3.

The Johnson Cook plasticity model, summarized in equation (63), is addressed first. Initial values for Kirchhoff stress τ^n, inverse plastic right Cauchy-Green tensor, $\mathbf{C}^{p-1\,n}$ and equivalent plastic strain $\bar{\varepsilon}^n$ are available at time t^n and τ^{n+1}, $\mathbf{C}^{p-1\,n+1}$ and $\bar{\varepsilon}^{n+1}$ are the solutions sought at time t^{n+1}. First, a trial state is evaluated with the use of equations (42)-(47). The plastic yield function is evaluated at the trial state as $F^{tr} = F(\tau^{tr}, \bar{\varepsilon}^n)$. If $F^{tr} < 0$, then the elastic material state update is performed using equation (48). If $F^{tr} >= 0$, then plastic flow must evolve in order to satisfy the time-discretized system of equations in (63). These equations are

$$
\begin{aligned}
&F(\tau^{n+1},\bar{\varepsilon}^{n+1}) = \bar{\tau}^{n+1} - \left[A + B(\bar{\varepsilon}^{n+1})^N\right]\left[1 + C\ln\left(\tfrac{\Delta\bar{\varepsilon}}{\Delta t}\right)\right]\left[1 - \left(\theta^{n+1}\right)^M\right] = 0 \\
&\tau^{n+1} = \frac{\partial\Psi}{\partial\varepsilon^e}(\varepsilon^{en+1}) \\
&\varepsilon^{en+1} = \varepsilon^{etr} - \Delta\lambda\left(\frac{\partial F}{\partial\tau}\right)^{n+1} \\
&\Delta\bar{\varepsilon} = \Delta\lambda h^{n+1} \\
&\bar{\varepsilon}^{n+1} = \bar{\varepsilon}^n + \Delta\bar{\varepsilon}
\end{aligned}
\tag{71}
$$

where

$$
\theta^{n+1} = \frac{T^{n+1} - T_r}{T_M - T_r} \tag{72}
$$

and the current temperature T^{n+1} is assumed to be known.

Next, the discrete equations for the Johnson Cook damage model, summarized in equation (70), are presented. Initial values for Kirchhoff stress τ^n, inverse plastic right Cauchy-Green tensor, $\mathbf{C}^{p-1\,n}$, equivalent plastic strain $\bar{\varepsilon}^n$ and damage D^n are available at time t^n. The values of τ^{n+1}, $\mathbf{C}^{p-1\,n+1}$, $\bar{\varepsilon}^{n+1}$ and D^{n+1} are the desired solutions. The trial state computation of $F^{tr} = F(\tau^{tr},\bar{\varepsilon}^n,D^n)$ is preformed in the same manner described above for the plasticity case. If $F^{tr} >= 0$, then plastic deformation and damage must evolve in order to satisfy the time-discretized system of equations in (70). The set of equations to be solved depends on the value of the trial triaxial condition σ^{*tr}, computed as follows:

$$
\sigma^{*tr} = \frac{p^{tr}}{\bar{\sigma}^{tr}} \tag{73}
$$

The equation set is

$$F(\tau^{n+1},\bar{\varepsilon}^{n+1},D^{n+1}) = \bar{\tau}^{n+1} - (1-D^{n+1})\left[A+B(\bar{\varepsilon}^{n+1})^N\right]\left[1+C\ln\left(\frac{\Delta\bar{\varepsilon}}{\Delta t}\right)\right]\left[1-\left(\theta^{n+1}\right)^M\right] = 0$$

$$\tau^{n+1} = \begin{cases} \left(\dfrac{\partial\Psi^{vol}}{\partial\varepsilon^e}\right)^{n+1} + (1-D^{n+1})\left(\dfrac{\partial\Psi^{dev}}{\partial\varepsilon^e}\right)^{n+1} & \sigma^{*tr} < 1.5 \\ (1-D^{n+1})\left(\dfrac{\partial\Psi}{\partial\varepsilon^e}\right)^{n+1} & \sigma^{*tr} \geq 1.5 \end{cases}$$

$$\varepsilon^{en+1} = \varepsilon^{etr} - \Delta\lambda\left(\frac{\partial F}{\partial\tau}\right)^{n+1}$$

$$\Delta\bar{\varepsilon} = \Delta\lambda h^{n+1}$$

$$\bar{\varepsilon}^{n+1} = \bar{\varepsilon}^n + \Delta\bar{\varepsilon}$$

$$\Delta D = \begin{cases} \Delta\bar{\varepsilon}\left(\left[D_1 + D_2 e^{D_3\sigma^{*n+1}}\right]\left[1+D_4\ln\left(\dfrac{\Delta\bar{\varepsilon}}{\Delta t\dot{\bar{\varepsilon}}_0}\right)\right]\left[1+D_5\theta^{n+1}\right]\right)^{-1} & \sigma^{*tr} < 1.5 \\ \dfrac{\Delta\bar{\varepsilon}}{\varepsilon^f_{min}} & \sigma^{*tr} \geq 1.5 \end{cases}$$

$$D^{n+1} = D^n + \Delta D \tag{74}$$

Newton's method is used to solve the nonlinear systems of equations describing the discrete finite strain Johnson Cook plasticity and damage models in equations (71) and (74) respectively. The systems to be solved are relatively small if full advantage of elastic plastic isotropy is taken (see Section 3). The plasticity model in (71) has seven equations and the damage model in equation (74) has eight equations. Once solutions are obtained, the updated $\mathbf{C}^{p-1\,n+1}$ is computed from equations (56)-(57) and the updated σ^{n+1} is obtained from equation (58). The remaining computational considerations are specific to the host code, ALEGRA, and are discussed next.

4.3 ALEGRA Implementation

The discrete finite strain Johnson Cook plasticity and damage models presented in Section 3 are implemented into the ALEGRA finite element shock and multi-physics code [3, 4]. The ALEGRA constitutive model interface requires more implementation considerations than a typical Lagrangian finite element code owing mostly to its Eulerian motion representation capability that is used extensively to simulate dynamic large deformation applications with multiple materials.

Three ALEGRA-specific issues are identified that must be addressed during the implementation of any constitutive model; availability of kinematic quantities, proper treatment of remapped history variables and proper treatment of material expansion.

An Eulerian ALEGRA simulation allows material motion through a fixed finite element mesh that represents the discretization of space. This motion is achieved through remap transport algorithms of material quantities [15]. A single Eulerian computational step (time step) is a two-step process that consists of a Lagrangian computation [16] to update quantities at time t^{n+1}, followed by a remap step that transports material quantities through the fixed grid. Not all material quantities are remapped. Once the remap operation is complete, certain material quantities are reevaluated in order to achieve a state that is consistent with quantities that are transported via remap. In the case of dynamic solid mechanics, the material quantities of interest to be remapped are the material density ρ^{n+1}, $\mathbf{V}^{n+1}$, $\mathbf{R}^{n+1}$, σ^{n+1}, and the history variables, which in this case of material modeled with the finite strain Johnson Cook model, are $\mathbf{C}^{p-1\,n+1}$, $\bar{\varepsilon}^{n+1}$ and D^{n+1}. A tilde is used to denote any quantity that has been remapped and an arrow $\longrightarrow$ is used to represent a remap operation as illustrated below for density.

$$\rho^{n+1} \underbrace{\longrightarrow}_{\text{remap operation}} \tilde{\rho}^{n+1} \tag{75}$$

The remap transport of scalar valued quantities such as ρ^{n+1}, $\bar{\varepsilon}^{n+1}$ and D^{n+1} are well understood and established operations [15]. However, ambiguity arises regarding the appropriate remapping of second order tensor quantities such as $\mathbf{V}^{n+1}$, $\mathbf{R}^{n+1}$, $\mathbf{C}^{p-1\,n+1}$ and σ^{n+1}. Presently, a component by component scalar remap scheme is utilized in ALEGRA for second order tensors. A suitable approach has been demonstrated tor the treatment of the kinematic quantities, $\mathbf{V}^{n+1}$ and $\mathbf{R}^{n+1}$, in a component-based remap approach [17]. The approach itself dictates the remap of $\mathbf{V}^{n+1}$ and $\mathbf{R}^{n+1}$ rather then attempting to remap $\mathbf{F}^{n+1}$. Introduction of finite strain plasticity into ALEGRA introduces the issue of remapping the tensor-valued history variable, $\mathbf{C}^{p-1\,n+1}$, which is symmetric positive definite (has real positive eigenvalues) and subject to the following isochoric plasticity constraint that follows from equation (13).

$$\det\left(\mathbf{C}^{p-1\,n+1}\right) = 1 \tag{76}$$

A special remap treatment of $\mathbf{C}^{p-1\,n+1}$ is proposed for the implementation of the the finite strain Johnson Cook model that is loosely based on the work in [18]. The approach is a component-based remap of the natural log of $\mathbf{C}^{p-1\,n+1}$ outlined in the series of operations presented below.

$$
\begin{aligned}
&\mathbf{A} = \ln\left(\mathbf{C}^{p-1\,n+1}\right) \\
&\mathbf{A} \underbrace{\longrightarrow}_{\text{remap operation}} \tilde{\mathbf{A}} \\
&\tilde{\mathbf{A}}^* = \tilde{\mathbf{A}} - \frac{1}{3} tr\left(\tilde{\mathbf{A}}\right) \\
&\tilde{\mathbf{C}}^{p-1\,n+1} = \exp\left(\tilde{\mathbf{A}}^*\right)
\end{aligned}
\tag{77}
$$

The remap of the natural log of $\mathbf{C}^{p-1\,n+1}$ and subsequent exponentiation ensures a positive definite result for $\tilde{\mathbf{C}}^{p-1\,n+1}$. The third operation in the series displayed in (77) is necessary to enforce the isochoric constraint in equation (76). While this extra operation does satisfy the necessary constraint, it amounts to a post-remap loss of kinematic information, for which the solution quality impact has not been carefully studied.

Remap of σ^{n+1} in ALEGRA has been preformed for all solid constitutive models up to this point. In the case of the finite strain Johnson Cook model, σ^{n+1} is not remapped, but reevaluated as $\tilde{\sigma}^{n+1}$, in order to be consistent with the remapped kinematic quantities $\tilde{\mathbf{V}}^{n+1}$, $\tilde{\mathbf{R}}^{n+1}$ and $\tilde{\mathbf{C}}^{p-1\,n+1}$. The evaluation is

$$
\tilde{\sigma}^{n+1} = \frac{1}{J^{n+1}} \frac{\partial \Psi}{\partial \varepsilon^e}(\tilde{\varepsilon}^{e\,n+1}) \tag{78}
$$

where

$$
\tilde{\varepsilon}^{e\,n+1} = \frac{1}{2} \ln(\tilde{\mathbf{b}}^{e\,n+1}) \tag{79}
$$

$$
\tilde{\mathbf{b}}^{e\,n+1} = \tilde{\mathbf{F}}^{n+1} \cdot \tilde{\mathbf{C}}^{p-1\,n} \cdot \tilde{\mathbf{F}}^{n+1\,T} \tag{80}
$$

and $\tilde{\mathbf{F}}^{n+1} = \tilde{\mathbf{V}}^{n+1} \cdot \tilde{\mathbf{R}}^{n+1}$.

The choice to use $\mathbf{C}^{p-1}$ as the tensor-valued plasticity history variable that is stored and transported is based on the availability of kinematic information at the ALEGRA constitutive model interface. Evaluation of the finite strain Johnson Cook model requires $\mathbf{b}^{e\,tr}$, which is typically obtained from equation (44) as follows.

$$
\mathbf{b}^{e\,tr} = \Delta\mathbf{F} \cdot \mathbf{b}^{e\,n} \cdot \Delta\mathbf{F}^T
$$

Since the incremental deformation gradient update, $\Delta\mathbf{F}$, is not computed in ALEGRA, the following alternative evaluation form of $\mathbf{b}^{e\,tr}$ from equation (45) is utilized:

$$\mathbf{b}^{etr} = \mathbf{F}^{n+1} \cdot \mathbf{C}^{p-1\,n} \cdot \mathbf{F}^{n+1\,T}$$

Since the updated deformation gradient is easily constructed as $\mathbf{F}^{n+1} = \mathbf{V}^{n+1} \cdot \mathbf{R}^{n+1}$, it is simply more convenient to use $\mathbf{C}^{p-1}$ as the plastic strain history variable.

Since ALEGRA is an explicit dynamics code, a stable time step must be computed every computational cycle. In general, the time step must satisfy the CFL condition for stability. The condition is

$$\Delta t = \beta \frac{\Delta x}{c} \tag{81}$$

where the CFL factor β is bounded according to $0 < \beta \leq 1$, Δx is a characteristic element length and the speed of sound in the material, c, is

$$c = \sqrt{\frac{K}{\rho}} \tag{82}$$

where K is the bulk modulus. The density is computed based on the conservation of mass. In the present case, K is approximated based on the hyperelastic model as follows:

$$K \approx \frac{\partial^2 \Psi^{vol}}{\partial (J^e)^2} \tag{83}$$

The mitigation of excessive material expansion is an important consideration founded on both physical and practical computational bases. Allowing separation of damaged material is not only physically intuitive, but prevents the inevitable time step crash $(\Delta t \longrightarrow 0)$ associated with a very low density material that has been allowed to expand unphysically. Consider the following definition of volumetric strain at time t^{n+1}.

$$\varepsilon_v^{n+1} = \ln(J^{n+1}) \tag{84}$$

An alternative representation of J^{n+1} in terms of density is

$$J^{n+1} = \frac{\rho^0}{\rho^{n+1}} \tag{85}$$

where ρ^0 is the initial density of the material at time $t^0 = 0$. The maximum allowable volumetric strain parameter, ε_v^{max} is introduced into the model and equations (84)-(85) are combined in order to obtain a minimum allowable density as follows:

$$\rho^{min} = \rho^0 e^{-\varepsilon_v^{max}} \tag{86}$$

If $D^{n+1} = 1$ and $\rho^{n+1} < \rho^{min}$ then $\rho^{n+1} = \rho^{min}$ is set. The effect of such a density modification in ALEGRA is a recalculation of the volume fractions of material, including void (empty space), on a per cell basis in order to satisfy conservation of mass. Consequently, the volume fraction of void increases as the damaged material tries to expand and the increase in volume of empty space allows damaged material to separate. Enforcing the density floor, ρ^{min}, can also prevent very small time steps due to very distended material.

Additional features of the ALEGRA implementation of the finite strain Johnson Cook model includes various algorithmic and model input options. An infinitesimal (small strain) formulation of the model has also been implemented in order to support a basic legacy Johnson Cook capability for combined models (see [4] for details). Any equation of state model implemented into ALEGRA can also be used as a sub-model with Johnson Cook. All model parameters can be specified individually or the user has the option of simply specifying any material available in the existing pre-defined Johnson Cook material parameter database. Usage of the finite strain Jonson Cook model in ALEGRA is documented in the ALEGRA user's manual [4].

5 ALEGRA Simulations

ALEGRA simulation results for problems utilizing the finite strain Johnson Cook constitutive model are presented in this section. First, simple deformation driven loading paths are evaluated for both plasticity and damage using a single Lagrangian 3D hexahedral element. Simulation results from the dynamic Taylor anvil impact problem are compared to experimental data. Localized deformation due to damage and fragmentation is then demonstrated by an expanding ring problem. Finally, results from an exploding cylinder application are presented.

All simulation results presented in the following sections utilizes the Neo Hookean hyperelastic Hemholtz energy form in equation (25), which is restated below.

$$\Psi(\mathbf{b}^e) = \frac{\kappa}{2}\left(\frac{1}{2}(J^{e\,2}-1) - \ln(J^e)\right) + \frac{\mu}{2}\left(\bar{\mathbf{b}}^e : \mathbf{I} - 3\right)$$

The verification testing conducted for this hyperelastic model in ALEGRA is the same as that performed for the LAME implementation [19]. All simulation results reflect isothermal and rate-independent behavior of the Johnson Cook model, for which $T = T_r = 298K\,(\theta = 0)$, $C = 0$ and $D_4 = 0$.

5.1 Lagrangian Single Element Simulations

Deformation driven loading paths are evaluated in ALEGRA for both plasticity and damage by applying prescribed deformations to a single Lagrangian 3D hexahedral element. The deformation is prescribed incrementally as follows:

$$\mathbf{F}^{n+1} = \Delta\mathbf{F} \cdot \mathbf{F}^n \tag{87}$$

The positive index $n = 0, 1, 2, \ldots, n_{max}$ in equation (87) denotes time step or cycle, for which $\mathbf{F}^0 = \mathbf{I}$, and an incremental deformation gradient, $\Delta\mathbf{F}$, is prescribed. Uniaxial strain and simple shear loading paths are evaluated. The value of $\Delta\mathbf{F}$ for uniaxial strain is

$$\Delta\mathbf{F} = \begin{pmatrix} 1 \pm \gamma & 0 & 0 \\ 0 & 1 & 0 \\ 0 & 0 & 1 \end{pmatrix} \tag{88}$$

where $+\gamma$ and $-\gamma$ represent extension and compression respectively. The value of $\Delta\mathbf{F}$ for simple shear is

$$\Delta \mathbf{F} = \begin{pmatrix} 1 & \gamma & 0 \\ 0 & 1 & 0 \\ 0 & 0 & 1 \end{pmatrix} \tag{89}$$

The values of the prescribed deformation parameters are $n_{max} = 100$ and $\gamma = 0.01$. The single element is initially a cube with side length, $h = 1\,m$. Copper material parameters are utilized. The mass initial mass density is $\rho^0 = 8930\,kg/m^3$. Elastic parameters are $\kappa = 200\,GPa$ and $\mu = 75\,GPa$. The Johnson Cook plasticity and damage model parameters taken from [2] are $A = 89.7\,MPa$, $B = 291.87\,MPa$, $N = 0.31$, $D_1 = 0.54$, $D_2 = 4.89$ and $D_3 = -3.03$. The minimum failure strain, obtained from equation (67), is $\varepsilon^f_{min} = 0.59$.

Results of the single element simulations are displayed in Figures 1 and 2. Each set of results contains load path representations in stress invariant space, $-P - \sqrt{J_2}$, where $\sqrt{J_2} = \sqrt{3}\bar{\sigma}$ and stretch vs. stress component space, $V_{xx} - \sigma_{xx}$ or $V_{xy} - \sigma_{xy}$. Stored elastic energy history and $\bar{\varepsilon}$ evolution are also included. The equivalent plastic strain evolution for the case of plasticity is nearly identical for uniaxial strain in tension and compression (lower left Figure 1). If the damage model is evaluated, the evolution of $\bar{\varepsilon}$ for uniaxial tension and compression paths is very different. The material becomes completely damaged ($D = 1$ indicated by the constant value of $\bar{\varepsilon}$) in the case of uniaxial tension, while no noticeable damage evolution occurs for uniaxial compression. This result is apparent from the loading paths and stored energy history plots of Figure 1. Spall failure is activated for the tensile loading path, which eventually drives σ_{xx}, P and $\sqrt{J_2}$ to zero. Consequently, the stored elastic energy decreases to zero. Since almost no damage accumulates for compression, the stress and energy histories of the plasticity and damage models are indistinguishable. Such a result is expected due to the relatively high failure strains, ε^f, predicted for negative values of the triaxial ratio, σ^*, produced in compression. In contrast, the tensile loading path utilizes a constant failure strain allowing for the evolution of completely damaged material with continued loading.

The simple shear loading path, displayed in Figure 2, is also associated with a constant failure strain value due to a zero value of σ^* (zero value of P). Damage does evolve for the shear loading path, indicated by the lower values of stress and stored energy, however the evolution of damage is restricted by the relatively high value of ε^f associated with the loading path.

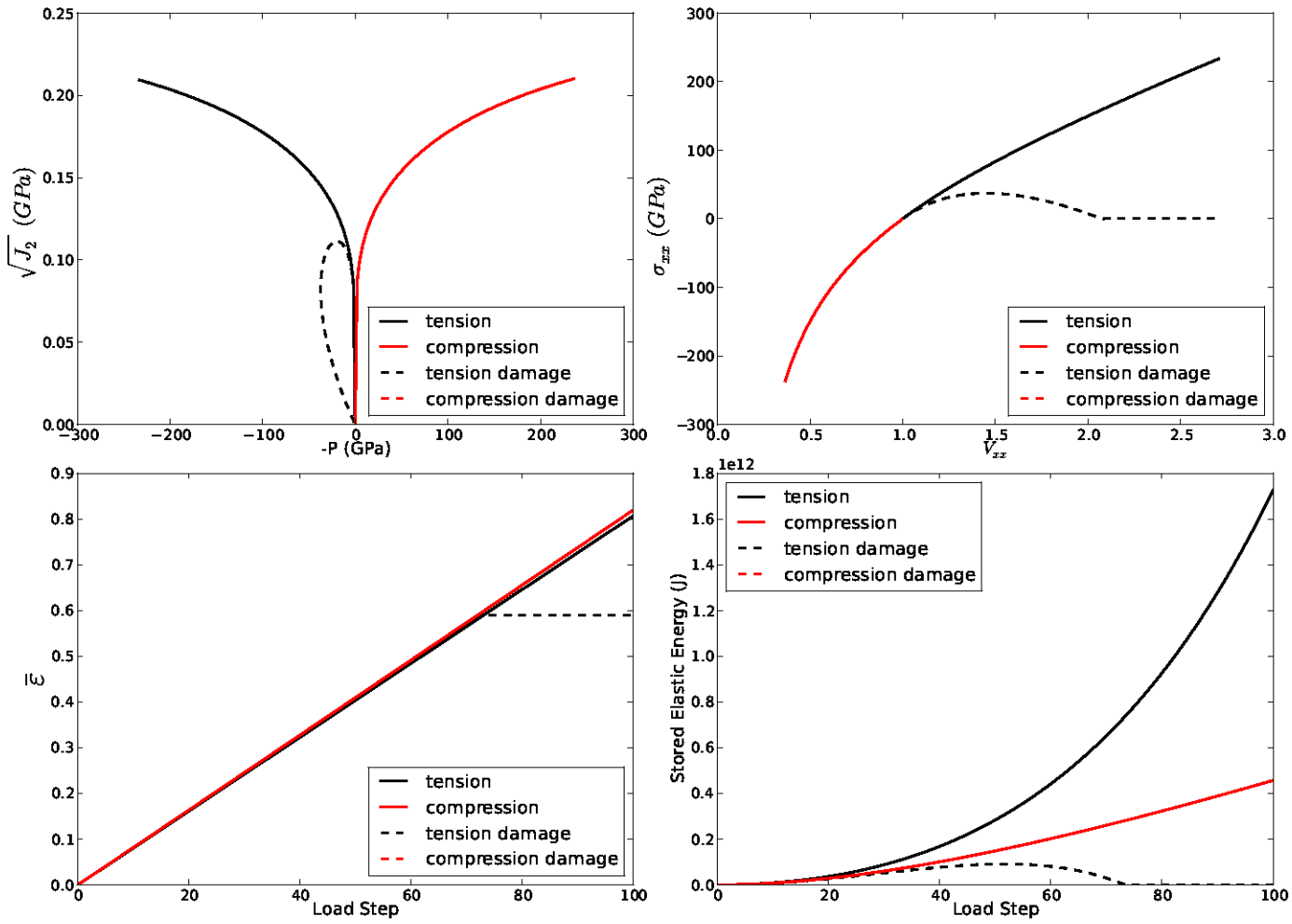

Figure 1. Finite strain Johnson Cook model: uniaxial strain

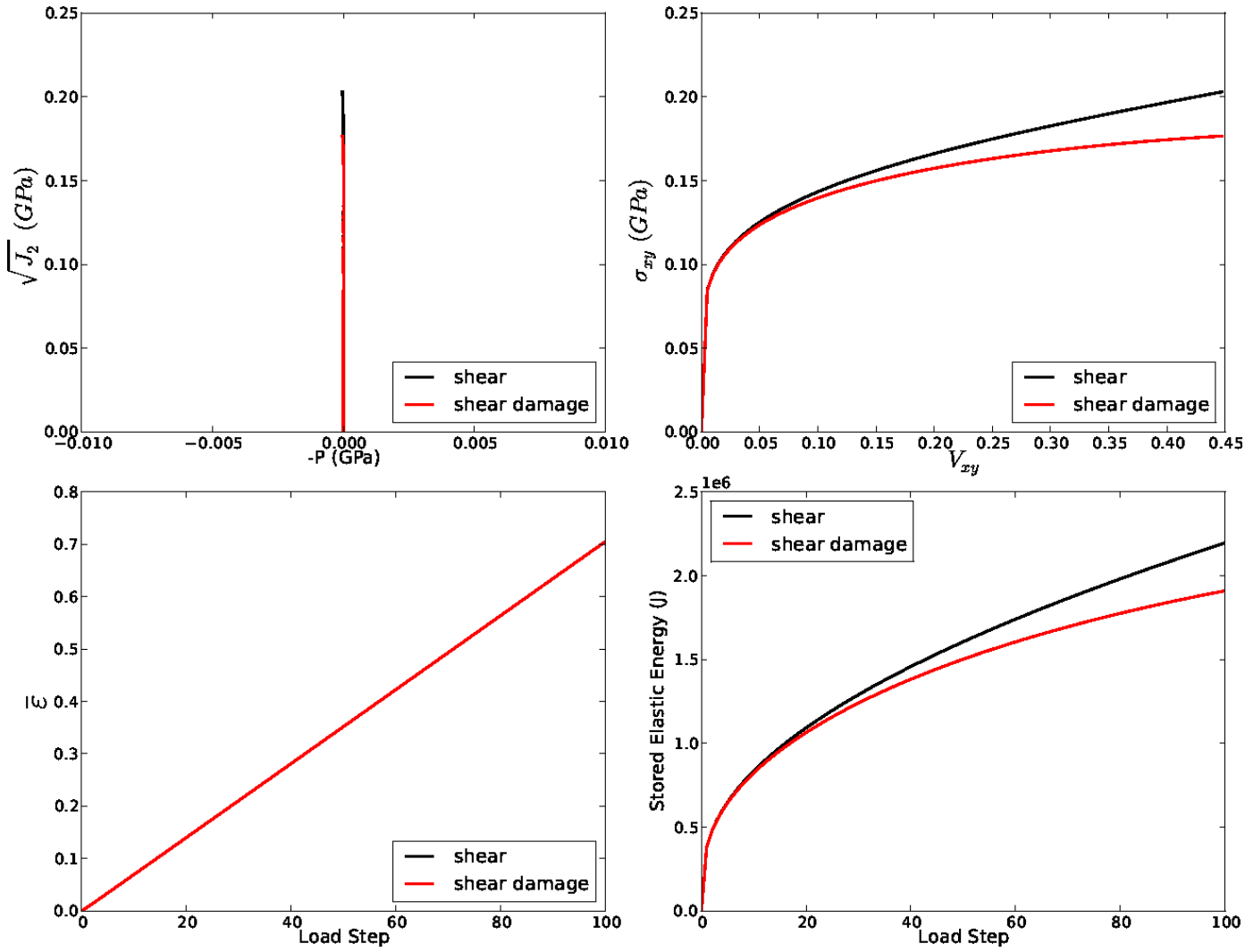

Figure 2. Finite strain Johnson Cook model: simple shear

5.2 The Taylor Anvil

The Taylor cylinder experiment [20] is simulated using the finite strain Johnson Cook plasticity model in ALEGRA . This dynamic test, illustrated in Figure 3, consists of a cylinder impacting a rigid surface at some initial velocity v_0. The numerical analysis follows that performed by Lacy et. al. [14]. In their work, the Taylor impact problem is used to assess the solution quality of several codes (including ALEGRA) by observing how well the simulations reproduce the experimental deformation result [13]. The same basic comparison is performed in the present work.

The description of the problem is taken directly from [14] which is based on the experiments performed in [13]. The two dimensional axisymmetric cylinder geometry depicted in Figure 3 is described by an initial radius $R = 0.381\,cm$ and height $H = 2.54\,cm$. The initial velocity of the cylinder is $v_0 = 19000\,cm/s$. The copper material parameter values are the same as those used in Section 5.1.

Taylor anvil ALEGRA simulation comparisons with experimental data are displayed in Figures 4 - 6. Each set of plots displays the initial configuration at $t = 0$ (left plot) and the final configuration at $t = 80\,\mu s$ (right plot). The finial configurations are overlaid on experimental deformed test specimen profile data taken from [14]. Qualitative agreement between the test data and simulations is observed for Lagrangian, Eulerian and Lagrangian material tracer (LMT) (see reference [21]) simulations displayed in Figures 4, 5 and 6 respectively.

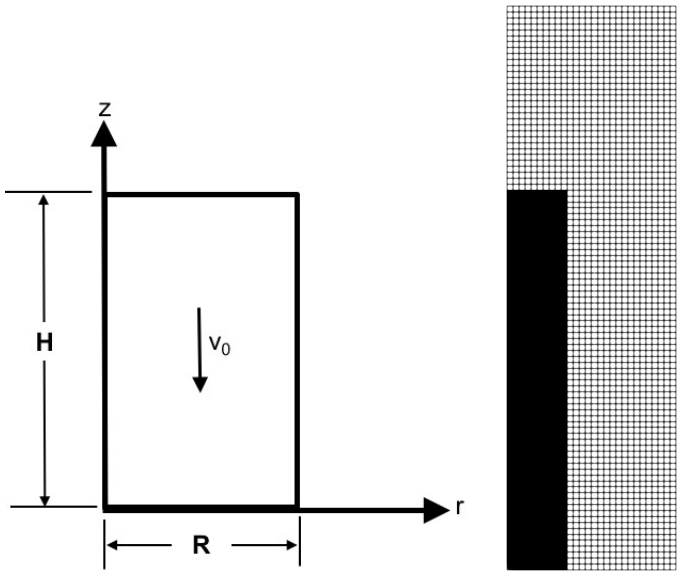

Figure 3. Taylor anvil problem definition (left) and initial configuration in Eulerian mesh (right)

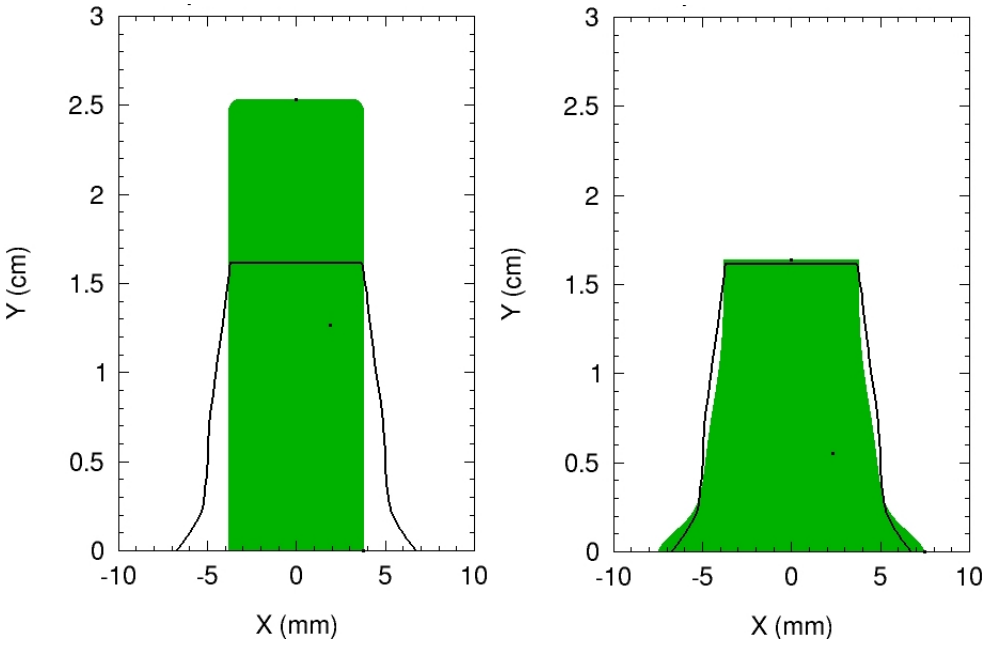

Figure 4. Lagrangian Taylor anvil ALEGRA simulation.

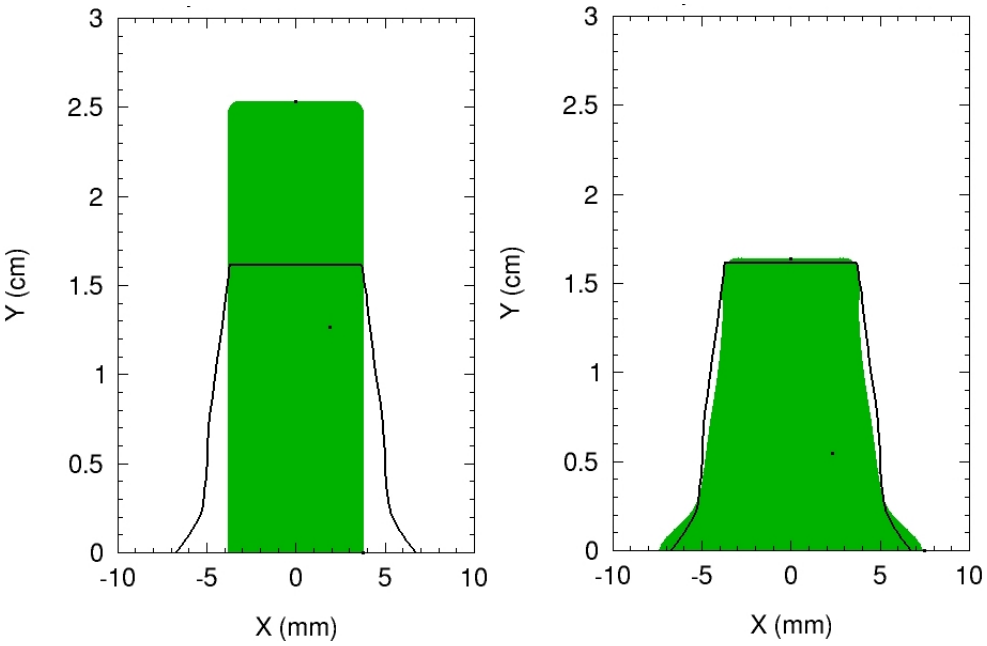

Figure 5. Eulerian Taylor anvil ALEGRA simulation.

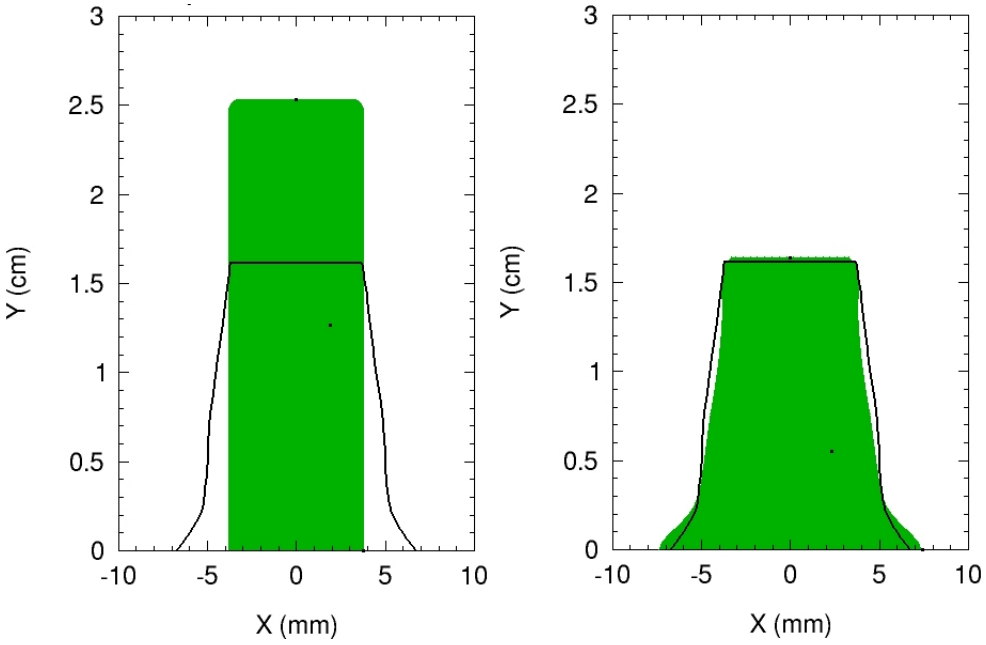

Figure 6. Eulerian LMT Taylor anvil ALEGRA simulation.

5.3 The Expanding Ring

The localized deformation and fragmentation of an expanding ring subjected to a uniform radial body force is simulated in ALEGRA. This problem is based on experiments performed by Benson and Grady [22], in which uniform tensile load is applied to the ring using an electromagnetic field. The thin aluminum ring has an outer diameter of $32mm$ and a $1mm \times 1mm$ square cross section. Experimental results show that material failure of the ring due to circumferential tension is preceded by ductile necking of the ring cross section which are localized at relatively even spaced locations along the ring's circumference.

Aluminum material parameters are utilized. The mass initial mass density is $\rho^0 = 2787\,kg/m^3$. Elastic parameters are $\kappa = 80.2\,GPa$ and $\mu = 30.5\,GPa$. The Johnson Cook plasticity and damage model parameters are $A = 265\,MPa$, $B = 426.42\,MPa$, $N = 0.34$, $D_1 = 0.13$, $D_2 = 0.13$ and $D_3 = -1.5$. The minimum failure strain, obtained from equation (67), is $\varepsilon^f_{min} = 0.143$. In addition, a maximum volumetric strain parameter value, $\varepsilon_v^{max} = 0.1$ is also prescribed (see Section 4.3).

The localized failure of a geometrically uniform structure subjected to spatially uniform loading is attributed to inhomogeneity in the material. In order to capture this feature of failure of real materials, a statistical approach is utilized, for which the aleatory uncertainty (uncertainty in spatial variation) and size effect of A are considered (see [23] and [24]). The value of the yield surface parameter, A which varies spatially, is taken from a Weibull probability distribution function with the following form:

$$A = \bar{A}\left(\frac{ln(R)}{ln\left(\frac{1}{2}\right)}\right)^{\frac{1}{m}} \tag{90}$$

The median value of A for aluminum is $\bar{A} = 265MPa$, the Weibull modulus is $m = 10$, and R is a random number from a uniform distribution ranging from 0 to 1. A plot of the resulting distribution is plotted in Figure 7.

The radial loading of the ring is simulated by the application of a prescribed body acceleration (external force) to the mesh nodes. The body acceleration field $\mathbf{a}(\mathbf{r},t)$ is applied to the mesh node radial positions $\mathbf{r}_i(t) = x_i\mathbf{e}_x + y_i\mathbf{e}_y$, where $\mathbf{e}_x$ and $\mathbf{e}_y$ are the global Cartesian unit basis vectors and (x_i, y_i, z_i) are the corresponding cartesian coordinates of a node. The body acceleration function is

$$\mathbf{a} = a\left(-\frac{y_i}{r}\mathbf{e}_x + \frac{x_i}{r}\mathbf{e}_y\right) \tag{91}$$

where $r = \sqrt{x_i^2 + y_i^2}$ and $a = 1.15 \times 10^7\, m/s^2$.

Deformation results for Lagrangian and Eulerian representations of the expanding ring problem are displayed in Figures 8 and 9 respectively. The local damaged zones that form in the Lagrangian problem (Figures 8) are due to plastic necking that initiates locally based on the random spatial

variability of the yield surface parameter A. The same behavior is observed for the Eulerian case in Figure 9, but the material is permitted to separate into distinct fragments. The global energy histories for the simulations displayed in Figure 10 demonstrate an expected loss of the stored elastic energy due to the fragmentation of the ring. While the elastic energies predicted for the Lagrangian and Eulerian simulations appear to be similar, there is a very noticeable difference in the internal energy between the two results that occurs once the elastic stored energy is significantly reduced. It is possible that the dissipative nature of the remapping operation associated with the Eulerian computation contributes to this difference.

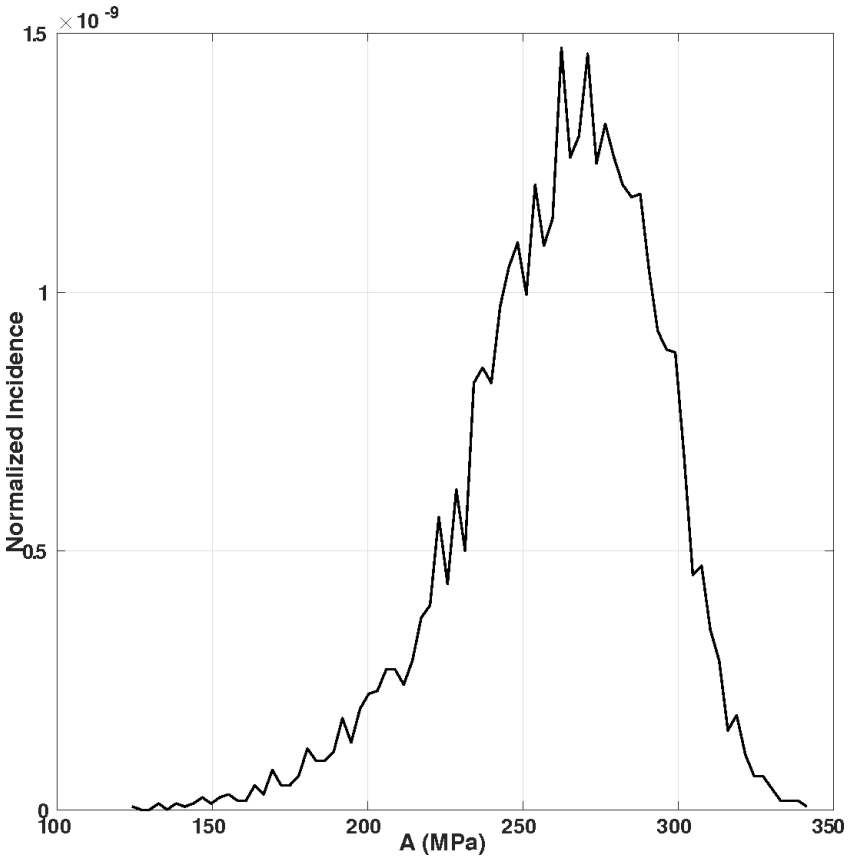

Figure 7. Distribution of yield strength A

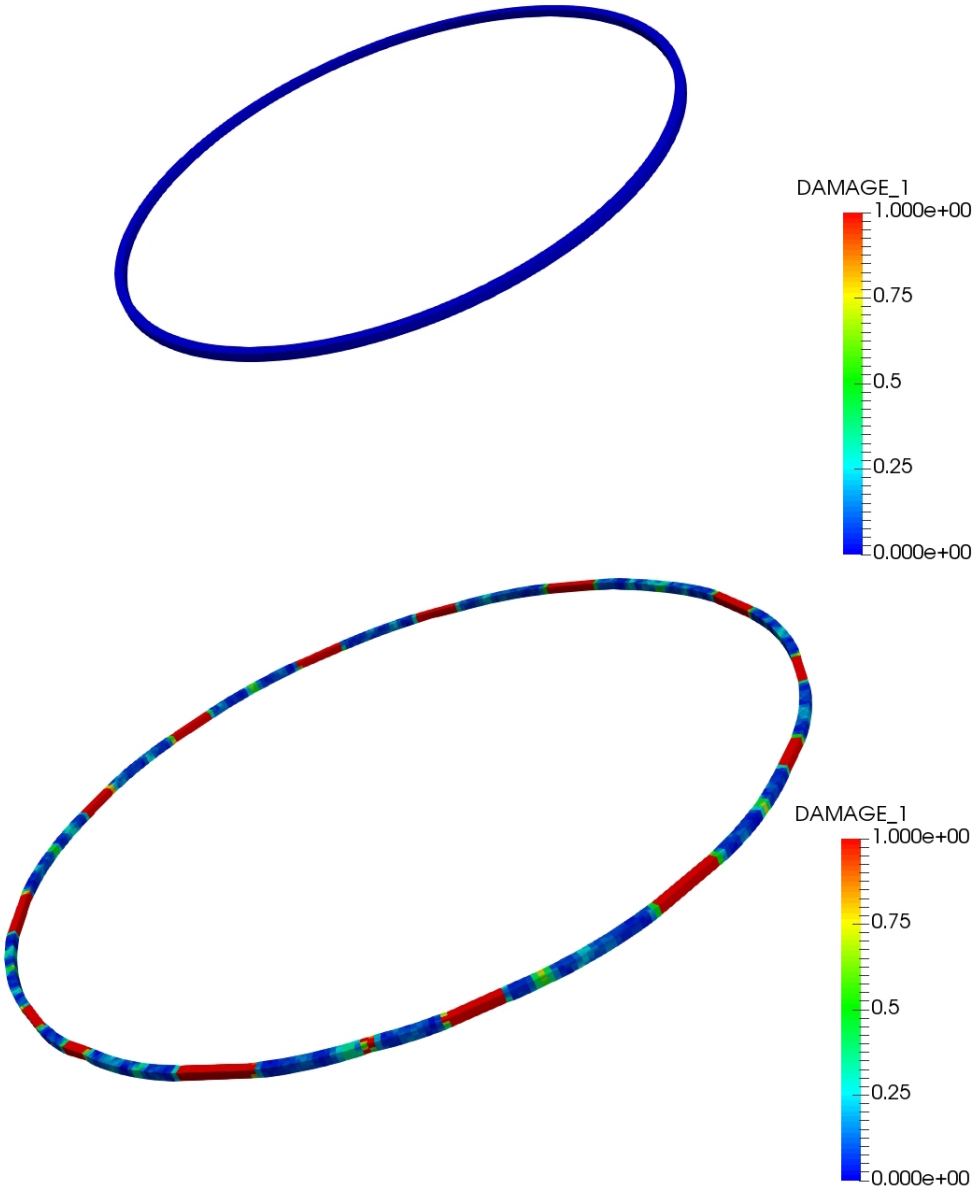

Figure 8. Lagrangian expanding ring ALEGRA simulation: $t = 0$ (top), $t = 50\mu s$ (bottom)

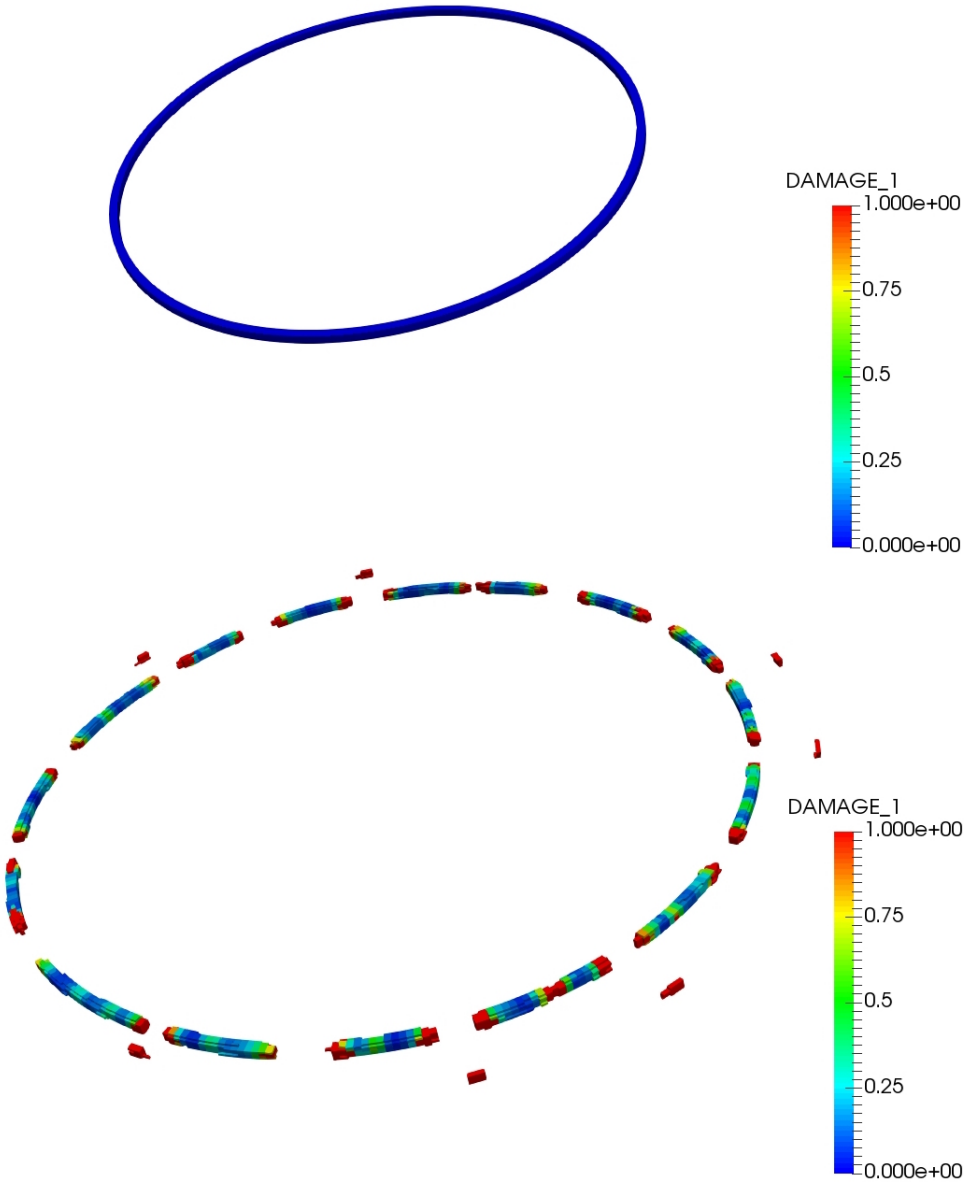

Figure 9. Eulerian expanding ring ALEGRA simulation: $t = 0$ (top), $t = 50\mu s$ (bottom)

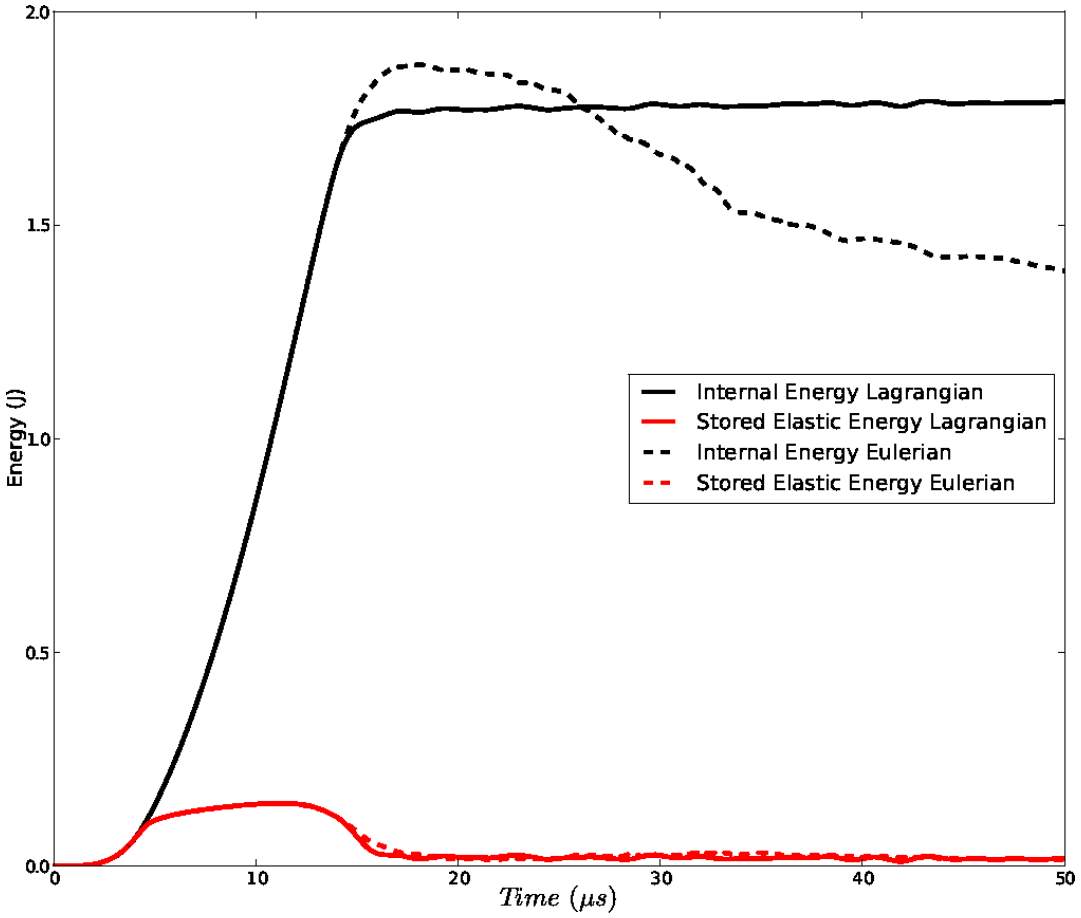

Figure 10. Expanding ring internal and elastic energy

5.4 The Exploding Cylinder

The fragmentation of a three dimensional hollow aluminum cylinder subjected to an internal detonation is simulated in ALEGRA. This problem is similar to the experimental work in [25]. The inner radius of the cylinder is $3.5\,cm$, the cylinder thickness is $5\,mm$ and the cylinder length is $20\,cm$. The Johnson Cook aluminum material parameter values are the same as those used in Section 5.3 including the Weibull probability distribution applied to the yield parameter A. Details of the explosive material inside the cylinder are omitted. A detonation is initiated at a concentric point located at one end of the cylinder.

Figures 11a - f display a progression of the fragmenting cylinder throughout the $30\,\mu s$ event. Each plot is colored according to damage. Only material that retains load carrying capacity is displayed ($D \leq 0.95$) in the plots. Restricting the visualization in this manner allows identification of solid material fragments.

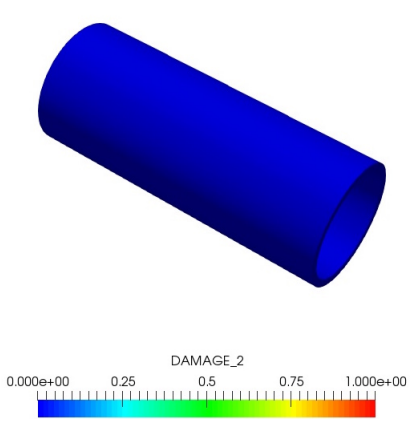

(a) $t = 0\mu s$

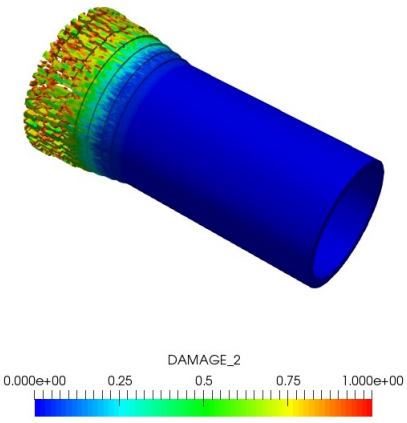

(b) $t = 10\mu s$

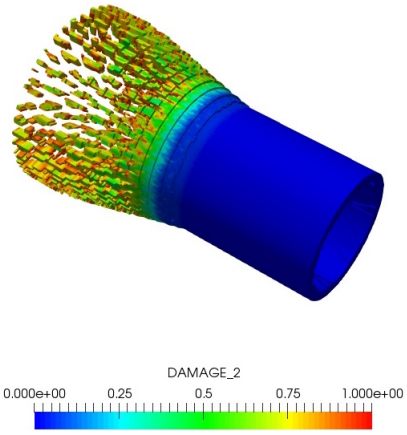

(c) $t = 15\mu s$

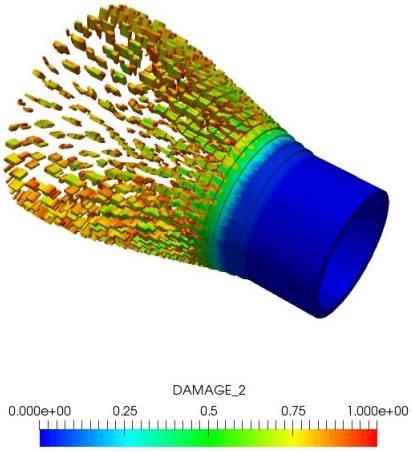

(d) $t = 20\mu s$

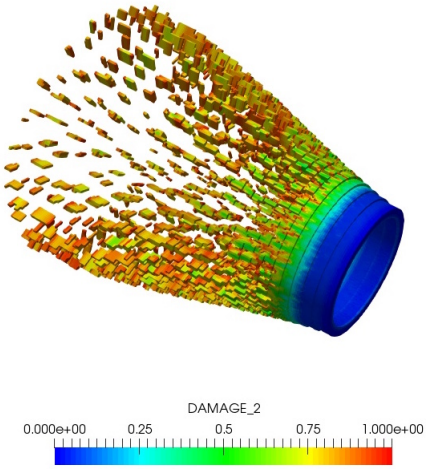

(e) $t = 25\mu s$

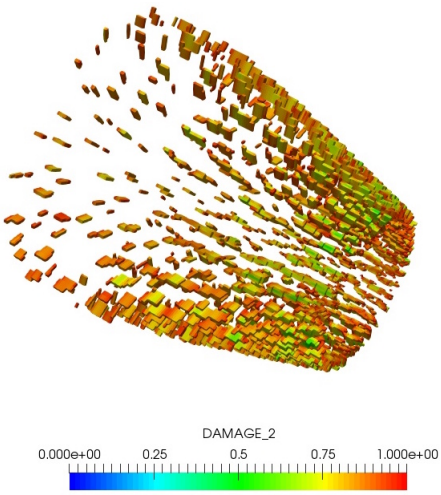

(f) $t = 30\mu s$

Figure 11. Exploding cylinder ALEGRA simulation

6 Conclusions & Future Work

A finite strain formulation of the Johnson Cook plasticity and damage model and its numerical implementation into the ALEGRA code has been presented. This implementation consists of a strong coupling of damage and the stored elastic energy as well as the minimum failure strain criterion for spall included in the original model development. The deformation driven loading paths demonstrated the basic features of the model using Johnson Cook parameterization for copper. A total loss of load carrying capacity and stored elastic energy is is the result for a spall failure activated in uniaxial tensile strain. In contrast, no noticeable damage occurs in uniaxial compressive strain. Use of the Johnson Cook finite strain plasticity model produces good comparisons with experimental Taylor anvil data. The model is applied to problems that incorporate material failure using random spatial variation of material parameters. Localized deformation leading to fragmentation is produced in the expanding ring problem while the global elastic stored energy is reduced to zero. The fragmentation of an exploding cylinder can be visualized by removing the completely damaged material, leaving behind intact solid fragments that are still able to carry load. The material failure simulations preformed for this work reproduce the qualitative nature of the experiments on which they are based.

This effort has laid down the necessary foundation for a thermodynamically consistent and complete continuum solid material model, for which all intensive properties derive from a common energy. The goal of developing such a model is to improve upon the shortcomings of ALEGRA's combined model framework discussed in Section 1. Presently, this work only addresses thermodynamic quantities associated with solid mechanics, such as stress and history variables. The introduction of thermodynamic quantities associated with the equation of state (for solids) still remains as future work that is important for shock and thermomechanical applications.

References

[1] G. Johnson and W. Cook. A constitutive model and data for metals subjected to large strains, high strain rates, and high temperatures. In *Proc. 7th Int. Symposium on Ballistics*, page 541, 1983.

[2] G. Johnson and W. Cook. Fracture characteristics of three metals subjected to various strains, strain rates, temperatures, and pressures. *Engineering Fracture Mechanics*, 21(1):31–48, 1985.

[3] A. C. Robinson et al. ALEGRA: An arbitrary Lagrangian-Eulerian multimaterial, multiphysics code. In *Proceedings of the 46th AIAA Aerospace Sciences Meeting*, Reno, Nevada, January 2008. AIAA-2008-1235.

[4] A.C. Robinson et al. Alegra user manual. Technical report SAND2014-1236, Sandia National Laboratories, Albuquerque, NM 87185, May 2014.

[5] W.M. Scherzinger. Anisotropic equation of state models. Memo SAND2017-4724 O, Sandia National Laboratories, Albuquerque, NM 87185, May 2017.

[6] C. Miehe. Entropic thermoelasticity at finite strains. aspects of the formulation and numerical implementation. *Computer Methods in Applied Mechanics and Engineering*, 120:243–269, 1995.

[7] K.Y. Kim. Thermodynamics at finite deformation of an anisotropic elastic solid. *Physical Review B*, 54:6245–6254, 1996.

[8] V.A. Lubarda. Constitutive theories based on the multiplicative decomposition of deformation gradient: Thermoelasticity, elastoplasticity, and biomechanics. *Appl. Mech. Rev.*, 57:95–108, 2004.

[9] A.A. Lukyanov. An equation of state for anisotropic solids under shock loading. *The European Physical Journal B*, 64:159–164, 2008.

[10] A.W. Hammer and S. Hartmann. Theoretical and numerical aspects in weak-compressible finite strain thermo-elasticity. *Journal of Theoretical and Applied Mechanics*, 50:3–22, 2012.

[11] E.A. de Souza Neto, D. Peric, and D.R.J. Owen. *Computational Methods for Plasticity: Theory and Applications*. John Wiley & Sons, Ltd, Chichester, UK, 2008.

[12] J.C. Simo and T.J.R. Hughes. *Computational Inelasticity*. Springer-Verlag, New York, 1998.

[13] G.R. Johnson and T.J. Holmquist. Test data and computational strength and fracture model constants for 23 materials subjected to large strains, high strain rates and high temperatures. Technical Report LA-11463-MS, Los Alamos National Laboratories, 1989.

[14] J.M. Lacy , S.R. Novascone, W.D. Richins and T.K. Larson Idaho National Laboratory. *A Method for Selecting Software for Dynamic Event Analysis II: The Taylor Anvil and Dynamic Brazilian Tests*, Orlando, FL, USA, 2008. Proceedings of the 16th International Conference on Nuclear Engineering.

[15] J.S. Peery and D.E. Carroll. Multi-material ale methods in unstructured grids. *Computer Methods in Applied Mechanics and Engineering*, 187:591–619, 2000.

[16] E. Love and M.K. Wong. Lagrangian continuum dynamics in ALEGRA. Technical Report SAND2007-8104, Sandia National Laboratories, Albuquerque, NM, 2007.

[17] A.C. Robinson, D.I. Ketcheson, T.L. Ames, and G.V. Farnsworth. A comparison of lagrangian/eulerian approaches for tracking the kinematics of high deformation solid motion. Technical report SAND2009-5154, Sandia National Laboratories, Albuquerque, NM 87185, September 2009.

[18] A. Mota, W. Sun, J.T. Ostien, J.W. Foulk, and K.N. Long. Lie-group interpolation and variational recovery for internal variables. *Comput. Mech.*, 53:1281–1299, 2013.

[19] W.M. Scherzinger, B.T. Lester, and P. Newell. Library of advanced materials for engineering (lame) 4.40. Technical Report SAND2016-2774, Sandia National Laboratories, Albuquerque, NM 87185, March 2016.

[20] G.I. Taylor. The use of flat ended projectiles for determining yield stress, part i theoretical considerations. *Proceedings of the Royal Society (London)*, 194:289–299, 1948.

[21] J.J. Sanchez, C.B. Luchini, and O.E. Strack. Lagrangian material tracers (lmt) for simulating material damage in alegra. Technical Report SAND2016-7260, Sandia National Laboratories, Albuquerque, NM 87185, July 2016.

[22] D. Grady and D. Benson. Fragmentation of metal rings by electromagnetic loading. *Experimental Mechanics*, 23:393–400, 1983.

[23] J.E. Bishop and O.E. Strack. A statistical method for verifying mesh convergence in monte carlo simulations with application to fragmentation. *International Journal for Numerical Methods in Engineering*, 88:279–306, 2011.

[24] O.E. Strack, R.B. Leavy, and R.M. Brannon. Aleatory uncertainty and scale effects in computational damage models for failure and fragmentation. *International Journal for Numerical Methods in Engineering*, 102:468–495, 2015.

[25] D.M. Goto, R. Becker, T.J. Orzechowski, H.K. Springer, A.J. Sunwoo, and C.K. Syn. Investigation of the fractue and fragmentation of sxplosively driven rings and cylinders. *International Journal of Impact Engineering*, 35:1547–1556, 1948.

A Finite Strain Plastic Flow Time Integration

The key component of this solution algorithm is the time integration of the plastic flow evolution equation in (35), restated below for convenience.

$$\dot{\mathbf{F}}^{p} = \dot{\lambda}\,\mathbf{R}^{eT} \cdot \frac{\partial F}{\partial \tau} \cdot \mathbf{R}^{e} \cdot \mathbf{F}^{p}$$

Given the initial data, $\mathbf{F}^{pn}$, equation (35) is integrated over time increment $\Delta t = t^{n+1} - t^{n}$ using a backward (fully implicit) exponential map. The result is

$$\mathbf{F}^{pn+1} = \exp\left[\Delta t \dot{\lambda}\,\mathbf{R}^{eTn+1} \cdot \left(\frac{\partial F}{\partial \tau}\right)^{n+1} \cdot \mathbf{R}^{en+1}\right] \cdot \mathbf{F}^{pn} \tag{92}$$

Further simplification of equation (92) yields the following result.

$$\mathbf{F}^{pn+1} = \mathbf{R}^{eTn+1} \cdot \exp\left[\Delta\lambda \left(\frac{\partial F}{\partial \tau}\right)^{n+1}\right] \cdot \mathbf{R}^{en+1} \cdot \mathbf{F}^{pn} \tag{93}$$

The quantities $\mathbf{F}^{pn+1}$ and $\mathbf{F}^{pn}$ can be expressed alternatively using equations (2) and (41). The results are

$$\mathbf{F}^{pn+1} = \mathbf{F}^{e-1n+1} \cdot \Delta\mathbf{F} \cdot \mathbf{F}^{n} \tag{94}$$

and

$$\mathbf{F}^{pn} = \mathbf{F}^{e-1n} \cdot \mathbf{F}^{n} \tag{95}$$

Equations (93)-(95) are combined. The result is

$$\mathbf{F}^{e-1n+1} \cdot \Delta\mathbf{F} = \mathbf{R}^{eTn+1} \cdot \exp\left[\Delta\lambda \left(\frac{\partial F}{\partial \tau}\right)^{n+1}\right] \cdot \mathbf{R}^{en+1} \cdot \mathbf{F}^{e-1n} \tag{96}$$

After some rearrangement and use of equation (42), equation (96) becomes

$$\mathbf{F}^{en+1} = \mathbf{F}^{etr} \cdot \mathbf{R}^{eTn+1} \cdot \exp\left[-\Delta\lambda \left(\frac{\partial F}{\partial \tau}\right)^{n+1}\right] \cdot \mathbf{R}^{en+1} \tag{97}$$

Post multiplication of each side of equation (97) by $\mathbf{R}^{en+1T}$ and use of equation (4) gives the following result.

$$\mathbf{V}^{en+1} = \mathbf{F}^{etr} \cdot \mathbf{R}^{eTn+1} \cdot \exp\left[-\Delta\lambda \left(\frac{\partial F}{\partial \tau}\right)^{n+1}\right] \tag{98}$$

The exponential tensor is moved to the left hand side of equation (98).

$$\mathbf{V}^{en+1} \cdot \exp\left[\Delta\lambda \left(\frac{\partial F}{\partial \tau}\right)^{n+1}\right] = \mathbf{F}^{etr} \cdot \mathbf{R}^{eTn+1} \tag{99}$$

Each side of equation (99) is post multiplied by its transpose. The result is

$$\mathbf{V}^{en+1} \cdot \exp\left[2\Delta\lambda \left(\frac{\partial F}{\partial \tau}\right)^{n+1}\right] \cdot \mathbf{V}^{en+1} = \mathbf{V}^{etr} \cdot \mathbf{V}^{etr} \tag{100}$$

Use is made of equation (7) and the elastic plastic isotropy property in equation (39). Equation (100) becomes

$$\mathbf{b}^{en+1} = \mathbf{b}^{etr} \cdot \exp\left[-2\Delta\lambda \left(\frac{\partial F}{\partial \tau}\right)^{n+1}\right] \tag{101}$$

Taking the natural log of both sides of equation (101) and use of equation (11) results in the following expression for the plastic flow evolution.

$$\varepsilon^{en+1} = \varepsilon^{etr} - \Delta\lambda \left(\frac{\partial F}{\partial \tau}\right)^{n+1} \tag{102}$$

DISTRIBUTION:

1 R.L. Doney
U.S. Army Research Laboratory
ATTN: RDRL-WMP-D
Aberdeen Proving Ground, MD, 21005
(electronic copy)

1 R.B. Leavy
U.S. Army Research Laboratory
ATTN: RDRL-WMP-C
Aberdeen Proving Ground, MD, 21005
(electronic copy)

1 MS 1323 Glen Hansen (electronic copy), 01443
1 MS 1323 John Niederhaus (electronic copy), 01446
1 MS 1323 Allen Robinson (electronic copy), 01443
1 MS 1323 Jason Sanchez (electronic copy), 01443
1 MS 1323 Ed Love (electronic copy), 01443
1 MS 0840 William Scherzinger (electronic copy), 01554
1 MS 9042 Jakob Ostien (electronic copy), 08343
1 MS 1323 John Carpenter (electronic copy), 01444
1 MS 0840 Steve Attaway (electronic copy), 01555
1 MS 0840 Kevin Ruggirello (electronic copy), 01555
1 MS 0899 Technical Library (electronic copy), 9536

Sandia National Laboratories